Copyright Warning & Restrictions

The copyright law of the United States (Title 17, United States Code) governs the making of photocopies or other reproductions of copyrighted material.

Under certain conditions specified in the law, libraries and archives are authorized to furnish a photocopy or other reproduction. One of these specified conditions is that the photocopy or reproduction is not to be "used for any purpose other than private study, scholarship, or research." If a, user makes a request for, or later uses, a photocopy or reproduction for purposes in excess of "fair use" that user may be liable for copyright infringement,

This institution reserves the right to refuse to accept a copying order if, in its judgment, fulfillment of the order would involve violation of copyright law.

Please Note: The author retains the copyright while the New Jersey Institute of Technology reserves the right to distribute this thesis or dissertation

Printing note: If you do not wish to print this page, then select "Pages from: first page # to: last page #" on the print dialog screen

NJIT New Jersey's Science & Technology University

The Van Houten library has removed some of the personal information and all signatures from the approval page and biographical sketches of theses and dissertations in order to protect the identity of NJIT graduates and faculty.

ABSTRACT

SYSTEM DESIGN AND PERFORMANCE ANALYSIS OF ASYMMETRICALLY AND SYMMETRICALLY CLIPPED OPTICAL (ASCO)-OFDM FOR IM/DD OPTICAL WIRELESS COMMUNICATIONS

by
Nan Wu

As the quantity of mobile communication devices, such as cellphones, tablets, and laptops, dramatically increase, the demand for high speed wireless service has been growing. Optical wireless communications (OWCs), which offer unlimited transmission bandwidth, have received a lot of attention and been studied in recent decades. They can be an effective alternative to radio frequency communications (RFCs) for indoor high speed data transmission. Intensity modulation direct detection (IM/DD) is a simple way to realize the transmission of optical wireless signals in an indoor environment. Information data streams are modulated into the intensity of optical carriers and transmitted by light emitting diodes (LEDs). At the receiver, the instantaneous power of optical signals can be directly detected by photodiodes. Multipath distortion, especially in an indoor environment, caused by reflection from walls or furniture, severely affects the transmission quality of optical signals. Orthogonal frequency division multiplexing (OFDM) is a promising modulation technique and has been widely used to combat inter-symbol-interference (ISI) resulting from multipath propagation in RFCs. So far, the technique of OFDM has also been successfully applied into IM/DD optical wireless systems. In this dissertation, the author focuses on the system design and performance analysis of a novel power-efficient scheme based on OFDM for IM/DD OWCs. This dissertation is divided into four main sections.

In the first part, a novel power-efficient scheme, called asymmetrically and symmetrically clipped optical (ASCO)-OFDM, for intensity modulation direct detection (IM/DD) optical wireless systems is proposed. The average bit rate versus (vs.) normalized bandwidth and the optical power per bit of this novel scheme are expressed by a closed form, respectively. The symbol error rate (SER) performance is investigated when optical signals are transmitted in a flat fading channel. Simulation results show that this proposed scheme can achieve better performances in terms of both power efficiency and symbol error rate (SER) when the optical power of transmitted signals is limited.

In the second part, an improved receiving technique is applied into the conventional receiver of ASCO-OFDM to improve the SER performance. This technique can explore and reuse some useful information hidden in the received signals. The detection procedure is described in detail and the improved SER performances are presented for different constellation cases.

In the third part, the information rates of ADO-OFDM and ASCO-OFDM are obtained for an additive white Gaussian noise (AWGN) channel with an average transmitted optical power constraint.

In the last part, this novel power efficient scheme, ASCO-OFDM, is extended into two-dimensional (2D) IM/DD optical wireless systems. The theoretical analysis and simulation results show that this technique not only achieves high average bit rate, but reduces the Peak-to-average power ratio (PAPR) as well.

SYSTEM DESIGN AND PERFORMANCE ANALYSIS OF ASYMMETRICALLY AND SYMMETRICALLY CLIPPED OPTICAL (ASCO)-OFDM FOR IM/DD OPTICAL WIRELESS COMMUNICATIONS

by
Nan Wu

A Dissertation
Submitted to the Faculty of
New Jersey Institute of Technology
in Partial Fulfillment of the Requirements for the Degree of
Doctor of Philosophy in Computer Engineering

Helen and John C. Hartmann Department of
Electrical and Computer Engineering

May 2015

Copyright © 2015 by Nan Wu

ALL RIGHTS RESERVED

APPROVAL PAGE

SYSTEM DESIGN AND PERFORMANCE ANALYSIS OF ASYMMETRICALLY AND SYMMETRICALLY CLIPPED OPTICAL (ASCO)-OFDM FOR IM/DD OPTICAL WIRELESS COMMUNICATIONS

Nan Wu

Dr. Yeheskel Bar-Ness, Dissertation Advisor — Date
Distinguished Emeritus Professor of Electrical and Computer Engineering, NJIT

Dr. Alexander M. Haimovich, Committee Member — Date
Distinguished Professor of Electrical and Computer Engineering, NJIT

Dr. Ali Abdi, Committee Member — Date
Associate Professor of Electrical and Computer Engineering, NJIT

Dr. Osvaldo Simeone, Committee Member — Date
Associate Professor of Electrical and Computer Engineering, NJIT

Dr. Sarah Kate Wilson, Committee Member — Date
Associate Professor of Electrical Engineering, Santa Clara University, CA

BIOGRAPHICAL SKETCH

Author: Nan Wu

Degree: Doctor of Philosophy

Date: May 2015

Undergraduate and Graduate Education:

- Doctor of Philosophy in Electrical Engineering,
  New Jersey Institute of Technology, Newark, NJ, 2015

- Master of Science in Electrical Engineering,
  New Jersey Institute of Technology, Newark, NJ, 2011

- Bachelor of Science in Communication Engineering,
  Anhui Normal University, Wuhu, Anhui, P. R. China, 2009

Major: Electrical Engineering

Presentations and Publications:

N. Wu and Y. Bar-Ness, "A novel power-efficient scheme asymmetrically and symmetrically clipping optical (ASCO)-OFDM for IM/DD optical systems," *EURASIP Journal on Advances in Signal Processing* 2015: 3.

N. Wu and Y. Bar-Ness, "An improved performance decoding technique for asymmetrically and symmetrically clipped optical (ASCO)-OFDM," *the 48th Annual Asilomar Conference on Signals, Systems and Computers*, Monterey, CA, Nov. 2-5, 2014.

N. Wu and Y. Bar-Ness, "Lower bounds on the channel capacity of ASCO-OFDM and ADO-OFDM," *the 49th Annual Conference on Information Sciences and Systems*, Baltimore, MD, Mar. 18-20, 2015.

N. Wu and Y. Bar-Ness, "Performance of two-dimensional asymmetrically and symmetrically clipping optical OFDM in AWGN," *the 49th Annual Conference on Information Sciences and Systems*, Baltimore, MD, Mar. 18-20, 2015.

I dedicate this dissertation...

To my parents, Youping Wang (王佑萍) and Chengrong Wu (吴成荣),

for giving me life and endless love, for cultivating in me

the character of diligence and conscientiousness,

and for being the spiritual and moral guides for my life.

To my family, for their continuous care, support and

encouragement.

ACKNOWLEDGMENT

First and foremost, I would like to express my heartfelt gratitude to my advisor, Prof. Yeheskel Bar-Ness, who provided consistent supervision, valuable suggestion and warm encouragement during my PhD journey. It was a privilege to work with you these four years. All I learned from you are invaluable to my study and research and benefit me in the whole life.

I am deeply grateful to Prof. Alexander M. Haimovich for being my dissertation advisor after Prof. Yeheskel Bar-Ness became emeritus. Special thanks to my dissertation committee members: Prof. Osvaldo Simeone for sharing his knowledge when I request his help; Prof. Ali Abdi for providing the constructive comments about my work; Prof. Sarah Kate Wilson for enlarging my vision and providing me precious suggestion in my research area.

I want to thank my colleagues in the Elisha Yegal Bar-Ness Center for Wireless Communications and Signal Processing Research (CWCSPR): Eyal Katz, Amir Laufer, Yu Liu, Yueweng Wang, Erjian Zhang and all the others.

I also would like to express deep gratitude to Ms. Angela Retino for her enthusiastic assistance in every respect. My sincere gratitude also goes to all the people that assisted me during these years, especially Prof. Durgamadhab Misra, Prof. Janet M. Bodner, Ms. Jacinta Williams and Yanjia Sun.

TABLE OF CONTENTS

TABLE OF CONTENTS
(Continued)

Chapter **Page**

TABLE OF CONTENTS
(Continued)

Chapter **Page**

LIST OF TABLES

LIST OF FIGURES

LIST OF FIGURES
(Continued)

Figures **Page**

LIST OF ACRONYMS

RFCs	Radio Frequency Communications
OWCs	Optical Wireless Communications
IM/DD	Intensity Modulation/Direct Detection
AWGN	Additive White Gaussian Noise
OFDM	Orthogonal Frequency Division Multiplexing
IFFT/FFT	Inverse Fast Fourier Transform/ Fast Fourier Transform
CP	Cyclic Prefix
QAM	Quadrature Amplitude Modulation
PAM	Pulse Amplitude Modulation
MMSE	Minimum Mean Square Error
ZF	Zero Forcing
SER	Symbol Error Rate
SNR	Signal to Noise Ratio
PDF	Probability Density Function
CDF	Cumulative Distribution Function
PAPR	Peak-to-Average Power Ratio

CHAPTER 1

INTRODUCTION

1.1 Background and Objective

Due to the development of wireless communication, people can get access conveniently into wireless networks any time and any place to share information with their families and friends. However, the quantity of personal portable wireless communication devices has dramatically increased in recent years, and this issue is challenging the quality of high speed wireless data transmission service. Without any doubt, the frequency of using personal wireless devices in an indoor environment is much higher than that in an outdoor environment. Wi-Fi technology, which is an indoor application of radio frequency communications (RFCs), has been widely employed to provide a high quality indoor wireless data transmission service. Unfortunately, it is getting harder to satisfy the demand of increasing high speed data transmission because of limited spectral resources. Thus, optical wireless communications (OWCs), which have unlimited bandwidth, are considered as the next generation technique of indoor high speed wireless communication.

Intensity modulation direct detection (IM/DD) is a simple approach to implement indoor OWCs. The main difference between RFCs and OWCs is the carrier. Information data streams are modulated into electromagnetic waves and optical waves for RFCs and OWCs, respectively. The block diagram of a general indoor IM/DD optical wireless system is shown in Figure 1.1 [1]. Information is generated in the electrical domain so that all kinds of existing techniques can be used to process electrical signals. By using an electrical-to-optical converter, the information is modulated into the intensity of an optical carrier and transmitted through an optical channel. Correspondingly, an optical-to-

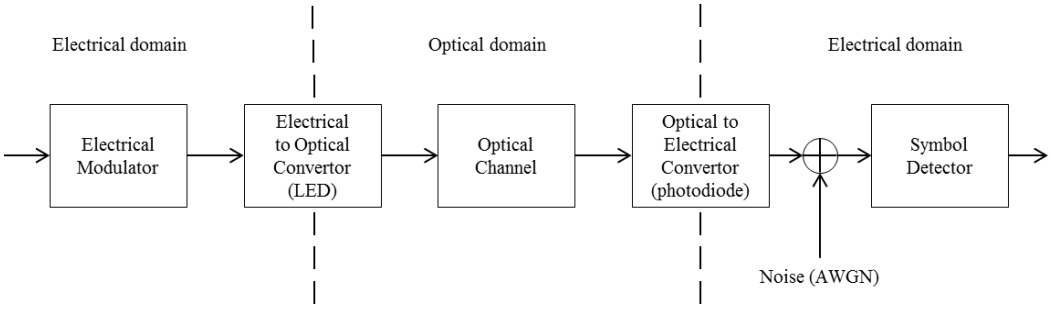

Figure 1.1 Block diagram of IM/DD optical wireless systems.

electrical converter is used to directly detect the instantaneous intensity of received optical signals. Finally, the transmitted information carried on the optical signals can be recovered in subsequent operations. In the described optical wireless system, the received optical signals are mainly distorted by two kinds of noises, ambient noise and thermal noise; the combination of these two noises can be modeled as additive white Gaussian noise (AWGN). An indoor optical wireless channel can be modeled as a multipath propagation channel [2]. The impulse response of this optical channel is shown as $h(t) = [h(0), h(1), \cdots, h(l)]$, where l is the number of channel coefficients. Multipath distortion, especially in an indoor environment, caused by reflection from walls or furniture, severely affects the transmission quality of an optical signal. Orthogonal Frequency Division Multiplexing (OFDM) [3] is a promising modulation technique and has been widely used to combat inter-symbol-interference (ISI) resulting from multipath propagation in RFCs. OFDM was studied for optical communications in [4]. So far, the schemes of optical OFDM have been successfully applied into IM/DD optical wireless systems, such as a DC-biased optical OFDM (DCO-OFDM) [5] and an asymmetrically clipped optical OFDM (ACO-OFDM) [6-7]. Combining the techniques of the previous two schemes, an asymmetrically clipped DC-biased optical OFDM (ADO-OFDM) [8] has been presented.

A light-emitting diode (LED), which is a two-lead semiconductor light source that converts voltage to light, can be adopted as a transmitter of optical wireless systems. When a modulated voltage is applied to the leads, the electrons will be recombined corresponding to the varying voltage, releasing energy in the form of photons. This effect is called electroluminescence. The transmitted information can be represented by the color of the light (corresponding to the intensity of the optical carrier). A photodiode that converts the light to current can be used to detect the received optical signal. Early LEDs have been used in infrared communications, transmitting low intensity infrared light. Meanwhile, LEDs will be widely used as novel indoor illumination devices because they have many advantages over incandescent light sources, including higher energy efficiency, longer lifetime, improved physical robustness, smaller size, and faster switching. The latest development in LEDs has made this application available. The high bright blue LEDs were invented by Japanese scientists, who were rewarded by the Nobel Prize in Physics last year. Combined with red and green LED lamps, the high bright white LED light source can be an alternative to the incandescent light source in the 21st century. LEDs will be extensively adopted to provide both illumination and communication in an indoor environment. However, the emitted light must obey eye safety regulations since high power light can be harmful to peoples' health, especially to their eyes. The scheme based on IM/DD optical wireless systems must be well-designed, offering higher data transmission with a constraint on transmitted optical power. Therefore, the criterion of power efficiency is quite important to optical wireless systems.

The objective of this dissertation is to comprehensively present a novel power efficient scheme, called asymmetrically and symmetrically clipped optical OFDM (ASCO-OFDM) [9], for IM/DD optical wireless communications. The system design and

performance analysis of this novel power-efficient scheme is sufficiently investigated and compared with another optical wireless system, asymmetrically clipped DC-biased optical OFDM (ADO-OFDM).

1.2 Optical Wireless Systems Overview

In this section, the two most popular OFDM-based IM/DD optical wireless systems will be briefly introduced. In IM/DD optical wireless systems, the information data streams are modulated into the intensity of optical carriers. Thus, only real and non-negative values can be used to realize the intensity modulation. Real signals can be obtained by applying an inverse fast Fourier transform (IFFT) to convert blocks of Hermitian symmetry complex symbols. A time domain signal sequence at the output of IFFT is shown in the middle of Figure 1.2. Note that it is real but bipolar. For the non-negative requirement of the transmitted optical signals, two mainstream approaches are extensively adopted, adding a DC bias and clipping. The resulted signals are separately shown on the two sides of Figure 1.2. The approach of adding a DC bias corresponds to the DC biased optical OFDM (DCO-OFDM) and clipping approach corresponds to the asymmetrically clipped optical OFDM (ACO-OFDM).

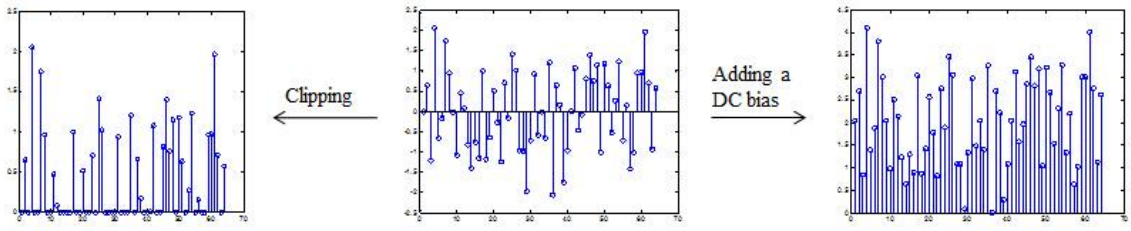

Figure 1.2 Two main approaches to make signals non-negative: Clipping (left) and Adding a DC bias (right).

1.2.1 DC Biased Optical (DCO)-OFDM

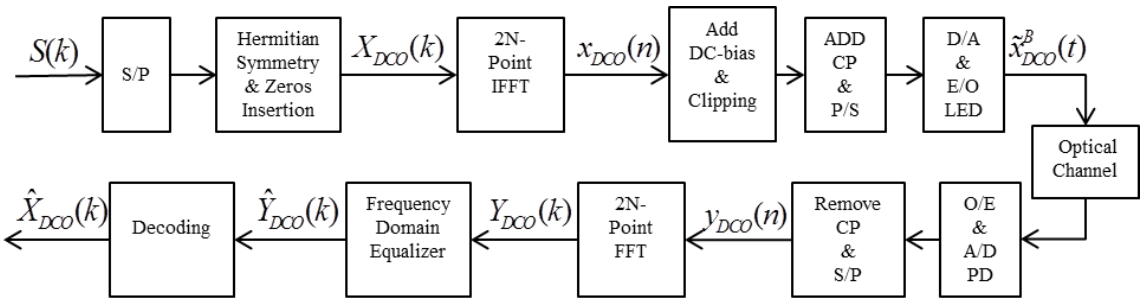

Figure 1.3 Block diagram of DC Biased Optical (DCO)-OFDM.

The block diagram of DC biased optical (DCO)-OFDM is shown in Figure 1.3. A signal vector of complex symbols $S(k)=[S_0,S_1,\cdots S_{N-2}]$ is input to the system of the DCO-OFDM modulation scheme. In order to obtain real signals, $S[k]$ has to be attached with its conjugate sequence in reverse order to yield a $(2N-2)\times 1$ vector $[S_0,S_1,\cdots S_{N-2},S_{N-2}^*,\cdots,S_1^*,S_0^*]^T$. Two zeroes are inserted into the first and the middle of the previous sequence to form a $2N\times 1$ Hermitian symmetry vector,

$$X_{DCO}(k)=[0,S_0,S_1,\cdots S_{N-2},0,S_{N-2}^*,\cdots,S_1^*,S_0^*]^T \tag{1.1}$$

A 2N-point IFFT is taken to construct the time domain signal vector $x_{DCO}(n)=[x_0,x_1,...,x_{2N-1}]^T$. Since $x_{DCO}(n)$ is real but bipolar, a suitable DC bias is then added to make it non-negative. Generally, the output of IFFT, $x_{DCO}(n)$, can be modeled as a block of Gaussian random variables with mean zero and variance $E\{x_{DCO}^2(n)\}$. The DC bias, B_{DC}, can be defined as the following: $B_{DC}=\mu\sqrt{E\{x_{DCO}^2(n)\}}$, where μ is a proportionality constant. The decibel form is given by $B_{DC(dB)}=10\log_{10}(\mu^2+1)dB$.

However, the DC bias cannot ensure all the elements in $x_{DCO}(n)$ non-negative, so the remaining negative values are clipped to zeroes, which result in clipping noise. In order to prevent clipping noise, a large DC bias should be added, but it makes the transmitted optical signal inefficient in terms of optical power. To avoid inter-carrier interference (ICI) as well as inter-block interference (IBI), a cyclic prefix (CP) of length l is appended to form $\tilde{x}_{DCO}(n)$. A DCO-OFDM transmitted signal is given by $\tilde{x}^{B}_{DCO}(n) = \tilde{x}_{DCO}(n) + B_{DC}$.

Since CP turns a linear convolution into a circular one, $\tilde{y}_{DCO}(n)$ serves as the circular convolution of $\tilde{x}^{B}_{DCO}(n)$ and $h(n)$, which is given by $\tilde{y}_{DCO}(n) = \tilde{x}^{B}_{DCO}(n) \otimes h(n) + w(n)$. $w(n)$ represents all kinds of interference, such as ambient noise and thermal noise. By using a photodiode, the received optical signal $\tilde{y}_{DCO}(n)$ is converted into the electrical domain, followed by the removal of the cyclic prefix in the following block to yield $y_{DCO}(n)$. It is assumed that the channel state information (CSI) is well known at the receiver. After passing into a 2N-point FFT, $Y_{DCO}(k)$ is operated by a single tap equalizer in the frequency domain. Finally, the information can be recovered by detecting the symbols in $\hat{Y}_{DCO}(k) = [0, Y_0, Y_1, \cdots, Y_{N-2}, 0, Y^*_{N-2}, \cdots, Y^*_1, Y^*_0]$.

1.2.2 Asymmetrically Clipped Optical (ACO)-OFDM

The block diagram of asymmetrically clipped optical (ACO)-OFDM is presented in Figure 1.4. A 2N-point IFFT will be used to construct ACO-OFDM signals with the same length as those of DCO-OFDM. A block of $(N/2-1)\times 1$ symbols is input to the

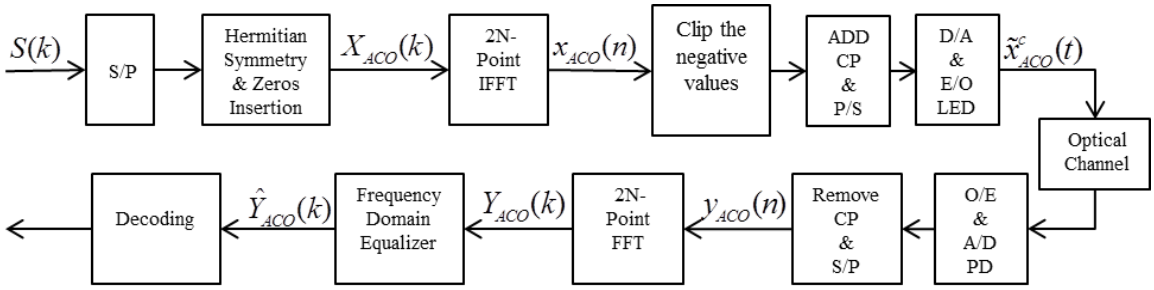

Figure 1.4 Block diagram of Asymmetrically Clipped Optical (ACO)-OFDM.

ACO-OFDM modulation scheme, which is given by $S(k)=[S_0,S_1,\cdots S_{N/2-1}]^T$. Then it will be combined with its conjugate sequence in reverse order to satisfy the Hermitian symmetry. However, these symbols are only mapped onto the odd subcarriers, and zeroes are set to the even subcarriers. The ACO-OFDM symbol vector is given by

$$X_{ACO}(k)=[0,S_0,0,S_1,0,\cdots 0,S_{N/2-1},0,S_{N/2-1}^*,0,\cdots 0,S_1^*,0,S_0^*]^T \tag{1.2}$$

Taken by a 2N-point IFFT into the time domain, the output is a $2N\times 1$ signal vector $x_{ACO}(n)=[x_0,x_1,...,x_{2N-1}]^T$. Due to the Hermitian symmetry, $x_{ACO}(n)$ is a real but bipolar signal. However, since each element in $x_{ACO}(n)$ is converted from odd subcarriers, this sequence has an asymmetrical relation that $x_{ACO}(n)=-x_{ACO}(n+N)$ where $n=0,1,\cdots,N-1$. Only non-negative values can be used to modulate the intensity of optical carriers, and all the negative elements in $x_{ACO}(n)$ have to be clipped to zeroes. The clipped ACO-OFDM signals are denoted by $x_{ACO}^c(n)$, which is given by $x_{ACO}^c(n)=0.5(x_{ACO}(n)+|x_{ACO}(n)|)$, where c indicates the clipping operation. Then, CP is attached to $x_{ACO}^c(n)$, which is denoted by $\tilde{x}_{ACO}^c(n)$, to mitigate the effect of inter-symbol

interference. After digital-to-analog convertor and electrical-to-optical convertor, $\tilde{x}_{ACO}^{c}(t)$ is transmitted by an LED through the channel $h(t)$. The arrival optical signal is detected by a photodiode, which is given by $\tilde{y}_{ACO}^{c}(t) = \tilde{x}_{ACO}^{c}(t) \otimes h(t) + w(t)$. The combination of all interference is approximated as Gaussian noise and it is given by $w(t)$.

At the receiver, the arrival optical signal is processed in reverse order to yield $y_{ACO}^{c}(n)$. $Y_{ACO}^{c}(k)$ is the 2N-point FFT of $y_{ACO}^{c}(n)$. After equalization, the detected ACO-OFDM signal vector is given by

$$\hat{Y}_{ACO}(k) = 0.5[C^0, S_0, C^1, S_2, ..., C^{N-2}, S_{N-2}, C^{N-3}, S_{N-2}^*, C^{N-4}, ..., S_2^*, C^{2N-1}, S_0^*]^T \quad (1.3)$$

The original symbols are still on the odd subcarriers but their amplitudes are reduced by half due to the clipping approach. Thus, the transmitted information can be recovered by extracting the odd component of $\hat{Y}_{ACO}(k)$, which is shown as follows $\hat{Y}_{ACO,odd}(k) = 0.5[0, S_0, 0, S_2, ..., 0, S_{N-2}, 0, S_{N-2}^*, 0, ..., S_2^*, 0, S_0^*]^T$. Some unknown symbols appear on the even subcarriers where should be zeroes. The even component of $\hat{Y}_{ACO}(k)$ is presented as follows:

$$\hat{Y}_{ACO,even}(k) = 0.5[C^0, 0, C^1, 0..., C^{N-2}, 0, C^{N-3}, 0, C^{N-4}, ..., 0, C^{2N-2}, 0]^T \quad (1.4)$$

These symbols are called ACO-OFDM clipping noise. Fortunately, ACO-OFDM clipping noise does not distort the original symbols. Moreover, it has been proved [10] that the clipping noise is the FFT of the scaled absolute version of $x_{ACO}(n)$, which is

given by $0.5|x_{ACO}(n)|$. Furthermore, the symbol error rate (SER) performance of ACO-OFDM achieves 3dB improvement by reusing the clipping noise in the decoding procedure. The improved performance receiving technique for the clipping OFDM optical system will be discussed in Chapter 3.

1.3 Outline of this Dissertation

This dissertation can be divided into five parts as follows:

1. The background of optical wireless communications and two typical IM/DD optical wireless systems based on the technique of OFDM, DCO-OFDM and ACO-OFDM, were reviewed in Chapter 1.

2. In Chapter 2, a novel power efficient scheme, asymmetrically and symmetrically clipped optical (ASCO)-OFDM is proposed.

3. In order to attain a better SER performance, an improved receiving technique for ASCO-OFDM is presented in Chapter 3.

4. The information rates of ASCO-OFDM in an AWGN channel with an optical transmitted power constraint are investigated in Chapter 4.

5. In Chapter 5, this power efficient scheme, ASCO-OFDM, is extended into two dimensional optical wireless systems.

CHAPTER 2

A NOVEL POWER-EFFICIENT SCHEME ASYMMETRICALLY AND SYMMETRICALLY CLIPPING OPTICAL (ASCO)-OFDM FOR IM/DD OPTICAL SYSTEMS

In Chapter 1, the principle of optical wireless systems has been introduced. Intensity modulation and direct detection (IM/DD) is a simple approach to be implemented in an indoor environment for optical wireless communications. Due to the inter-symbol interference (ISI) caused by multipath propagation, the promising technique, OFDM, is combined into IM/DD optical systems. Then, DCO-OFDM and ACO-OFDM, which correspond to adding a DC bias and clipping respectively, have been described in detail. In DCO-OFDM, a DC bias is added to eliminate the negative values in the transmitted signal. However, the performance of DCO-OFDM strongly depends on the DC bias level [11]. If the added DC bias cannot exceed the negative peak, the remaining negative values must be clipped to zero; then all subcarriers will be affected by the clipping noise. If the DC bias is larger than the negative peak, it makes the DCO-OFDM inefficient in terms of optical power. The advantage of DCO-OFDM is bandwidth efficiency because both odd and even subcarriers are used to carry data. In ACO-OFDM, all the negative values are clipped to zero, leaving the positives. In [12], the clipping approach reduces the amplitude of the original symbols by half, and the clipping noise falls onto the even subcarriers without distorting the data on the odd subcarriers. Thus, only odd subcarriers are used to carry data in ACO-OFDM. Compared to DCO-OFDM, ACO-OFDM is more optical power efficient but its bandwidth is twice that of DCO-OFDM.

In order to maintain the advantages and avoid the drawbacks of the previous two

optical systems, a combination scheme called ADO-OFDM has been designed. ACO-OFDM symbols modulate odd subcarriers while DCO-OFDM symbols modulate even subcarriers. The negative values generated by ACO-OFDM and DCO-OFDM are separately clipped to zero. Then the sum of the remaining two non-negative signals is transmitted by a light emitting diode (LED) [13-14]. ACO-OFDM symbols can be easily recovered by detecting the data carried on the odd subcarriers. The ACO-OFDM clipping noise can be estimated from the received ACO-OFDM signals. By adding a moderate DC bias at the transmitter, the clipping noise caused by DCO-OFDM is negligible compared to the wanted signal. Finally, DCO-OFDM symbols are successfully recovered by subtracting the estimated ACO-OFDM clipping noise from the received DCO-OFDM signals.

Adding a DC bias is a simple and direct approach, but it leads to a large waste of optical power. A full spectrally efficient optical system, hybrid ACO-OFDM [15], is proposed by Bilal Ranjha and Mohsen Kavehrad. Without using the DC bias, it is more power efficient than ADO-OFDM. The ideas for the system design of the hybrid ACO-OFDM and our proposed system are similar. For both, the odd subcarriers are used to carry ACO-OFDM symbols, which are drawn from quadrature amplitude modulation (QAM) constellations. The differences are that the hybrid ACO-OFDM uses the imaginary parts of the even subcarriers to carry PAM-DMT symbols, while we still map the QAM symbols onto the even subcarriers. We believe that our proposed system will be better than the hybrid ACO-OFDM because the average power of QAM symbols is much smaller than that of PAM symbols in the same level of constellation case.

So far, the Hermitian symmetry constraint is usually enforced on the signal vector for obtaining real signals. However, Hany Elgala and Thomas D. C. Little provided

another scheme, polar-OFDM (P-OFDM) [16], to generate real unipolar signals without this constraint. The QAM symbols are only mapped onto the even subcarriers. After taken by IFFT, the complex signal vector satisfies the half-wave even symmetry. Then, Hany Elgala and Thomas D. C. Little apply the Cartesian-to-Polar operation to convert the complex form into the exponential form. The amplitude and the phase values of different samples are transmitted. At the receiver, the authors use the reverse operation to recover the original complex symbols. The designing ideas of P-OFDM and our proposed system are quite different. The main difference depends on the use of the Hermitian symmetry constraint.

In this chapter, we propose a novel scheme, called an asymmetrically and symmetrically clipping optical (ASCO)-OFDM, to simultaneously transmit ACO-OFDM symbols on the odd subcarriers and symmetrically clipping optical SCO-OFDM symbols on the even subcarriers. If the length of an ACO-OFDM signal is 2N, an ACO-OFDM symbol that consists of only odd subcarriers has the property of $x(n) = -x(n+N)$ [12, 17]. However, an OFDM symbol converted from only even subcarriers satisfies the property that $x(n) = x(n+N)$, which is proved in Appendix A. After clipping, the same negative values are removed in the first and in the second half. It is the reason that the non-negative signals are called SCO-OFDM signals. Fortunately, the SCO-OFDM clipping noise does not affect ACO-OFDM symbols because it falls onto the even subcarriers. We prove this claim in Appendix B. By using the same operation in ADO-OFDM, we can recover ACO-OFDM symbols by extracting the data on the odd subcarriers. Also the ACO-OFDM clipping noise can be accurately estimated from the recovered ACO-OFDM signals. The data on the even subcarriers are distorted by the ACO-OFDM clipping noise, the SCO-OFDM clipping noise, and all other noises. The details of reconstructing SCO-

OFDM are discussed in section 2.2. Since no DC bias is added to all subcarriers, this novel scheme exhibits better performance in terms of optical power and symbol error rate (SER) than does ADO-OFDM.

2.1 Asymmetrically Clipped DC-Biased Optical (ADO)-OFDM

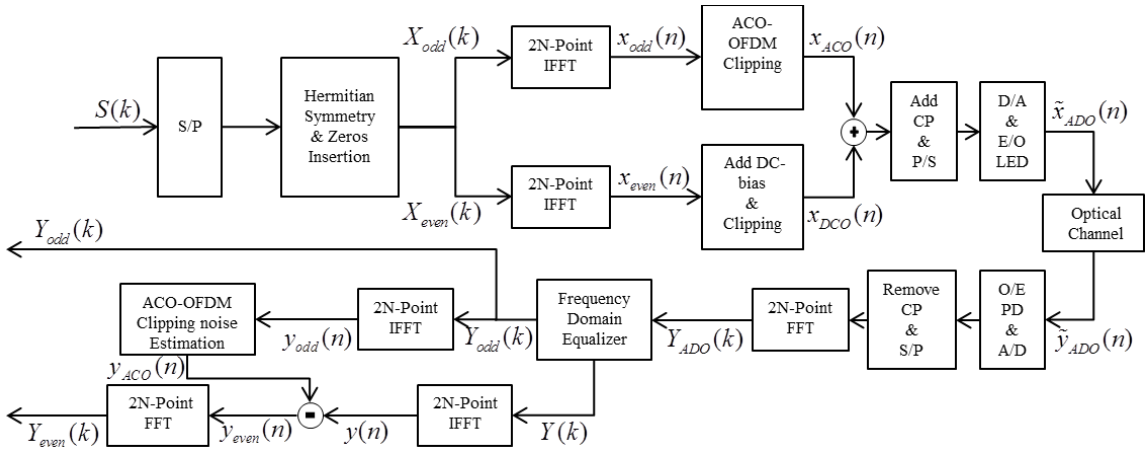

Figure 2.1 ADO-OFDM transmitter and receiver configuration.

Figure 2.1 shows the block diagram of ADO-OFDM. The input of the ADO-OFDM system is a block of $(N-1)\times 1$ complex data symbols $S=[S_0,S_1,...,S_{N-2}]^T$ mapped from constellations such as 4-QAM, 16-QAM, or 64-QAM. In order to obtain a real signal, this block of complex data symbols is combined with its conjugate sequence $S^*=[S_0^*,S_1^*,...,S_{N-2}^*]^T$ in reverse order to form a $2(N-1)\times 1$ signal vector that has Hermitian symmetry as follows, $[S_0,S_1,...,S_{N-2},S_{N-2}^*,...,S_1^*,S_0^*]^T$. Two zeroes are respectively inserted at the first and at the middle of this signal vector, which is shown as:

$$X=[0,S_0,S_1,...,S_{N-2},0,S_{N-2}^*,...,S_1^*,S_0^*]^T \tag{2.1}$$

Then X is divided into two $2N \times 1$ signal vectors, X_{odd} and X_{even}, that consist of the odd components and the even components of X, which are shown as:

$$X_{odd} = [0, S_0, 0, S_2 ..., 0, S_{N-2}, 0, S_{N-2}^*, 0, ..., S_2^*, 0, S_0^*]^T \tag{2.2}$$

$$X_{even} = [0, 0, S_1, 0, S_3 ..., S_{N-3}, 0, 0, 0, S_{N-3}^*, ..., S_3^*, 0, S_1^*, 0]^T \tag{2.3}$$

Both X_{odd} and X_{even} are converted by a 2N-point IFFT to yield two real bipolar signal vectors, x_{odd} and x_{even}, respectively. In an ACO-OFDM clipping block, the negative values in x_{odd} are clipped to zero to produce a signal, x_{ACO}, consisting of non-negative values. Another signal, x_{DCO}, is obtained by adding a DC bias to x_{even} and setting the remaining negative values to zero. In order to avoid the DCO-OFDM clipping noise, a large DC bias should be added which makes the transmitted optical signal inefficient in terms of optical power. Thus, the performance of DCO-OFDM depends on the bias level. Generally, x_{even} is modeled as a block of Gaussian random variables with mean zero and variance $E\{x_{even}^2\}$. The DC bias is denoted by B_{DC}, which can be defined as follows: $B_{DC} = \mu\sqrt{E\{x_{even}^2\}}$. $10\log_{10}(\mu^2 + 1)dB$ is the decibel form of B_{DC}, where μ is a proportionality constant. The transmitted signal $\tilde{x}_{ADO}$ is the sum of x_{ACO} and x_{DCO} with the cyclic prefix (CP) attached.

An indoor optical wireless channel can be modeled as a multipath propagation channel. The impulse response of this optical channel can be modeled as $h(t) = [h(0), h(1), \cdots, h(l)]$, where l is the number of channel coefficients which

determines the length of CP. At the receiver, a photodiode is employed to detect the intensity of the received optical signal:

$$\tilde{y}_{ADO}(n) = \tilde{x}_{ADO}(n) * h(n) + w(n) \tag{2.4}$$

which is the convolution of the incident optical signal and the optical channel plus noise. $w(n)$ represents the combination of shot noise and thermal noise, which can be approximated as additive white Gaussian noise. We assume that channel state information (CSI) is well-known at the receiver. The output of a 2N-point fast Fourier transform FFT, $Y_{ADO}(k)$, is operated by a single-tap equalizer in the frequency domain. X_{odd} can be recovered by extracting the odd component of Y followed by a hard or soft detection. By transforming Y_{odd} into the time domain, an ACO-OFDM clipping noise estimation block reconstructs a reference signal y_{ACO}. Finally, y_{DCO} is obtained by subtracting y_{ACO} from the reference signal y, and it is transformed into the frequency domain to yield Y_{even}.

2.2 Asymmetrically and Symmetrically Clipped Optical (ASCO)-OFDM

The block diagram of ASCO-OFDM is shown in Figure 2.2 Since the ASCO-OFDM system uses a novel transmission format, the input block of complex symbols is first separated into three parts, which have two $(N/2)\times 1$ signal vectors and one $(N/2-1)\times 1$ signal vector. Thus, the length of the input block is $3N/2-1$. Similarly, in order to obtain a real signal, we have to make the input of IFFT have the Hermitian symmetry. Two

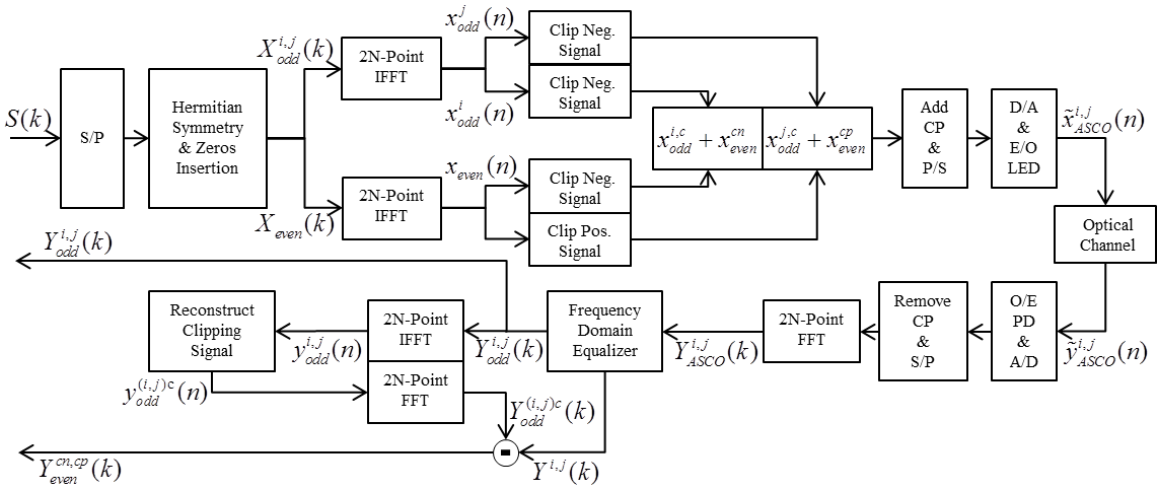

Figure 2.2 ASCO-OFDM transmitter and receiver configuration.

$(N/2)\times 1$ signal vectors are respectively combined with their conjugate sequences and are inserted by zeroes into the even subcarriers to form two $2N\times 1$ signal vectors, X_{odd}^{i} and X_{odd}^{j}, which are given by

$$X_{odd}^{i} = [0, S_0^i, 0, S_1^i ..., 0, S_{N/2}^i, 0, S_{N/2}^{i*}, 0, ..., S_1^{i*}, 0, S_0^{i*}]^T \tag{2.5}$$

$$X_{odd}^{j} = [0, S_0^j, 0, S_1^j ..., 0, S_{N/2}^j, 0, S_{N/2}^{j*}, 0, ..., S_1^{j*}, 0, S_0^{j*}]^T \tag{2.6}$$

The $(N/2-1)\times 1$ signal vector is defined in a similar way with zeroes inserted into the odd subcarrier to form a $2N\times 1$ signal vector X_{even} as follows:

$$X_{even} = [0, 0, S_0, 0, S_1 ..., S_{N/2-1}, 0, 0, 0, S_{N/2-1}^*, ..., S_1^*, 0, S_0^*, 0]^T \tag{2.7}$$

All three signal vectors X_{odd}^{i}, X_{odd}^{j}, and X_{even} are constrained to the Hermitian symmetry. They are taken by a 2N-point IFFT to produce real bipolar signal vectors x_{odd}^{i},

x_{odd}^{j}, and x_{even}, respectively. To ensure the non-negative requirement of the transmitted signals, all negative values in x_{odd}^{i} and x_{odd}^{j} are clipped to zero to generate $x_{odd}^{i,c}$ and $x_{odd}^{j,c}$, which are given by

$$x_{odd}^{i,c} = 0.5(x_{odd}^{i} + \left|x_{odd}^{i}\right|) \tag{2.8}$$

$$x_{odd}^{j,c} = 0.5(x_{odd}^{j} + \left|x_{odd}^{j}\right|) \tag{2.9}$$

As each sample in x_{even} is converted from even subcarriers, it has the relation that $x_{even}(n) = x_{even}(n+N)$. By clipping the negative values, half of the information carried in x_{even} is lost. Thus two signal vectors, x_{even}^{cn} and x_{even}^{cp}, are generated for transmitting the information in x_{even}. x_{even}^{cn} represents that all negative values of x_{even} are clipped to zero. x_{even}^{cp} represents that all positive values of x_{even} are clipped to zero and the remaining negative values are turned to positive. They are respectively given by:

$$x_{even}^{cn} = 0.5(x_{even} + \left|x_{even}\right|) \tag{2.10}$$

$$x_{even}^{cp} = 0.5(-x_{even} + \left|x_{even}\right|) \tag{2.11}$$

Then we construct a transmitted signal that consists of two consecutive sub-blocks, x_{ASCO}^{i} and x_{ASCO}^{j}, which is given by

$$x_{ASCO}^{i} = x_{odd}^{i,c} + x_{even}^{cn} = 0.5(x_{odd}^{i} + \left|x_{odd}^{i}\right| + x_{even} + \left|x_{even}\right|) \quad (2.12)$$

$$x_{ASCO}^{j} = x_{odd}^{j,c} + x_{even}^{cp} = 0.5(x_{odd}^{j} + \left|x_{odd}^{j}\right| - x_{even} + \left|x_{even}\right|) \quad (2.13)$$

The transmitted signals x_{ASCO}^{i} and x_{ASCO}^{j} with the cyclic prefix are denoted by $\tilde{x}_{ASCO}^{i}$ and $\tilde{x}_{ASCO}^{j}$. They are transmitted through an optical channel by an LED. The received signals $\tilde{y}_{ASCO}^{i}$ and $\tilde{y}_{ASCO}^{j}$ are given by

$$\tilde{y}_{ASCO}^{i}(n) = \tilde{x}_{ASCO}^{i}(n) * h(n) + w^{i}(n) \quad (2.14)$$

$$\tilde{y}_{ASCO}^{j}(n) = \tilde{x}_{ASCO}^{j}(n) * h(n) + w^{j}(n) \quad (2.15)$$

where the impulse response of optical channel $h(n)$ is modeled as $h(n) = [h(0), h(1), \cdots, h(l)]$, and the sum of all noise, $w^{i}(n)$ or $w^{j}(n)$, is approximately modeled as additive white Gaussian noise. After removing the cyclic prefix, the arrival signals, y_{ASCO}^{i} and y_{ASCO}^{j}, are respectively transformed by a 2N-point FFT into the frequency domain to yield Y_{ASCO}^{i} and Y_{ASCO}^{j}. Then, a frequency domain equalizer with the knowledge of channel state information is applied to Y_{ASCO}^{i} and Y_{ASCO}^{j} to yield:

$$Y^{i} = (\Lambda^{H}\Lambda + (\alpha / SNR)I_{2N})^{-1}\Lambda^{H}Y_{ASCO}^{i} \quad (2.16)$$

$$Y^{j} = (\Lambda^{H}\Lambda + (\alpha / SNR)I_{2N})^{-1}\Lambda^{H}Y_{ASCO}^{j} \quad (2.17)$$

where Λ is a $2N \times 2N$ diagonal matrix whose diagonal is the 2N-point FFT of $h(n)$, and Λ^H indicates the Hermitian matrix of Λ. The frequency domain equalizer can be a MMSE equalizer $(\alpha = 1)$ or a ZF equalizer $(\alpha = 0)$. Y^i and Y^j can also be shown in the frequency domain as follows,

$$\begin{aligned} Y^i &= X_{odd}^{i,c} + X_{even}^{cn} \\ &= 0.5(X_{odd}^i + \left|X_{odd}^i\right| + X_{even} + \left|X_{even}\right|) \end{aligned} \tag{2.18}$$

$$\begin{aligned} Y^j &= X_{odd}^{j,c} + X_{even}^{cp} \\ &= 0.5(X_{odd}^j + \left|X_{odd}^j\right| - X_{even} + \left|X_{even}\right|) \end{aligned} \tag{2.19}$$

where X_{odd}^i and $\left|X_{odd}^i\right|$ are the 2N-point FFT of x_{odd}^i and $\left|x_{odd}^i\right|$. The other corresponding terms in Equations (2.12), (2.13), (2.18), (2.19) are similarly defined. Note that the symbols of $0.5X_{odd}^i$ and $0.5X_{odd}^j$ fall onto the odd subcarriers of Y^i and Y^j, and the other symbols that consist of the remaining terms, $0.5(\left|X_{odd}^i\right| + X_{even} + \left|X_{even}\right|)$ and $0.5(\left|X_{odd}^j\right| - X_{even} + \left|X_{even}\right|)$, fall onto the even subcarriers of Y^i and Y^j, respectively. Thus, the complex symbols of X_{odd}^i and X_{odd}^j can be easily recovered by extracting the symbols of Y_{odd}^i and Y_{odd}^j, which are the odd components of Y^i and Y^j, because the clipping noise resulting from $x_{odd}^{i,c}$ and $x_{odd}^{j,c}$ only affects the even components of Y^i and Y^j. In order to accurately estimate the clipping noise, Y_{odd}^i and Y_{odd}^j are transformed into the time domain to yield two blocks of real bipolar signal y_{odd}^i and y_{odd}^j, respectively. $y_{odd}^{i,c}$ and $y_{odd}^{j,c}$ are two blocks of clipping reference signals which are generated in the same way as $x_{odd}^{i,c}$ and $x_{odd}^{j,c}$,

respectively; then, they are transformed back into the frequency domain to yield $Y_{odd}^{i,c}$ and $Y_{odd}^{j,c}$, respectively. Compared to Y_{odd}^{i} and Y_{odd}^{j}, $Y_{odd}^{i,c}$ and $Y_{odd}^{j,c}$ have the same symbol on the odd subcarriers, but the clipping noise appears on the even subcarriers. Therefore, Y_{even}^{cn} and Y_{even}^{cp} are obtained by subtracting $Y_{odd}^{i,c}$ and $Y_{odd}^{j,c}$ from Y^{i} and Y^{j}, respectively, which are given by

$$\begin{aligned} Y_{even}^{cn} &= Y^{i} - Y_{odd}^{i,c} \\ &= 0.5(X_{even} + |X_{even}|) \end{aligned} \tag{2.20}$$

$$\begin{aligned} Y_{even}^{cp} &= Y^{j} - Y_{odd}^{j,c} \\ &= 0.5(-X_{even} + |X_{even}|) \end{aligned} \tag{2.21}$$

We note that $x_{even} = x_{even}^{cn} - x_{even}^{cp}$; hence Y_{even} can be estimated by the form,

$$Y_{even} = Y_{even}^{cn} - Y_{even}^{cp} \tag{2.22}$$

2.3 Signal Analysis of ASCO-OFDM and ADO-OFDM

In this section, we first review the probability density function (PDF) of ADO-OFDM signals. Then the theoretical PDF of ASCO-OFDM signals is derived and two simulated PDF results are compared with the theoretical PDF in Figure 2.3. Moreover, we analyze the average bit rate/normalized bandwidth of ASCO-OFDM and ADO-OFDM. Through calculating the total optical power and the information bit of the transmitted signal, we obtain the optical power per bit for both schemes.

2.3.1 The Probability Density Function of ADO-OFDM and ASCO-OFDM

The PDF of ADO-OFDM signals is the convolution of the PDF of ACO-OFDM signals and the PDF of DCO-OFDM signals, which is given by Equation (2.28) in [8] because they have the relation that $x_{ADO}(n) = x_{ACO}(n) + x_{DCO}(n)$. The PDFs of ACO-OFDM signals and DCO-OFDM signals are respectively given by [2, 18-19],

$$f_{x_{ACO}(t)}(\chi) = \frac{1}{\sqrt{2\pi}\sigma_A} e^{\frac{-\chi^2}{2\sigma_A^2}} u(\chi) + \frac{1}{2}\delta(\chi) \tag{2.23}$$

$$f_{x_{DCO}(t)}(\chi) = \frac{1}{\sqrt{2\pi}\sigma_D} e^{\frac{-(\chi - B_{DC})^2}{2\sigma_D^2}} u(\chi) + Q(\frac{B_{DC}}{\sigma_D})\delta(\chi) \tag{2.24}$$

where $u(\chi)$ is unit step function and $\delta(\chi)$ is the Dirac delta function. σ_A is the standard deviation of the unclipped signal in ACO-OFDM, which is given by $\sigma_A = E\{x_{odd}^2\}$. σ_D is the standard deviation of DCO-OFDM signals, which is given by $\sigma_D = E\{x_{even}^2\}$. The PDF of ACO-OFDM signals is called clipped Gaussian distribution and it is only determined by σ_A. However, the PDF of DCO-OFDM signals is affected by σ_D and B_{DC}. Thus, the performance of ADO-OFDM partially depends on the DC bias level B_{DC}.

In the ASCO-OFDM modulation scheme, $x_{odd}^{i,c}$, $x_{odd}^{j,c}$, x_{even}^{cn} and x_{even}^{cp} are all real clipped signals. $x_{odd}^{i,c}$ and $x_{odd}^{j,c}$ are asymmetrically clipped (ACO-OFDM signals) while x_{even}^{cn} and x_{even}^{cp} are symmetrically clipped (SCO-OFDM signals). We assume that they all follow a Clipped Gaussian distribution, which is given by

$$f(x) = \frac{1}{\sqrt{2\pi}\sigma} e^{-\frac{x^2}{2\sigma^2}} u(x) + \frac{1}{2}\delta(x) \tag{2.25}$$

where σ is the standard deviation of the unclipped signal, such as x_{odd}^{i}, x_{odd}^{j} and x_{even}. Here we consider that x_{odd}^{i}, x_{odd}^{j} and x_{even} are modulated by the same constellation, so they have the same standard deviation σ. By using the clipped Gaussian distribution, we can obtain the PDF of ASCO-OFDM signals. Assuming $\alpha \in x_{odd}^{i,c}$ and $\beta \in x_{even}^{cn}$ $(\alpha, \beta \geq 0)$, $\chi = \alpha + \beta$ is the random variable of x_{ASCO}^{i}. The PDF of x_{ASCO}^{i} is the convolution of $f_{x_{odd}^{i,c}}(\alpha)$ and $f_{x_{even}^{cn}}(\beta)$, which is given by

$$f(\chi) = f_{x_{odd}^{i,c}}(\alpha) * f_{x_{even}^{cn}}(\beta) \tag{2.26}$$

where $f_{x_{odd}^{i,c}}(\alpha) = \frac{1}{\sqrt{2\pi}\sigma} e^{-\frac{\alpha^2}{2\sigma^2}} u(\alpha) + \frac{1}{2}\delta(\alpha)$ and $f_{x_{even}^{cn}}(\beta) = \frac{1}{\sqrt{2\pi}\sigma} e^{-\frac{\beta^2}{2\sigma^2}} u(\beta) + \frac{1}{2}\delta(\beta)$.

Thus, the PDF of x_{ASCO}^{i} is given by

$$f(\chi) = [\frac{1}{2\sqrt{\pi}\sigma} e^{-\frac{\chi^2}{4\sigma^2}} erf(\frac{\chi}{2\sigma}) + \frac{1}{\sqrt{2\pi}\sigma} e^{-\frac{\chi^2}{2\sigma^2}}] u(\chi) + \frac{1}{4}\delta(\chi) \tag{2.27}$$

with mean $2\sigma/\sqrt{2\pi}$ and variance $(\pi - 1)\sigma^2/\pi$. $erf(x)$ is the error function of x and the PDF curve is shown in Figure 2.3. The calculation steps of Equation 2.27 are shown in Appendix C.

The theoretical and simulated PDFs of ASCO-OFDM signals have been shown and compared in Figure 2.3. The theoretical result is given by Equation (2.27), which is the solid curve in the figure. Since the real bipolar signals at the output of an IFFT has a Gaussian distribution, we model x_{odd}^{i}, x_{odd}^{j} and x_{even} as Gaussian signals to generate the transmitted ASCO-OFDM signals. This simulated result is given by the plus solid curve. In order to obtain the PDF of signals generated by the ASCO-OFDM modulation scheme, we use a Monte Carlo experiment to get the statistical ASCO-OFDM signals. This simulated PDF is shown as a cross solid curve. Comparing these three curves, they closely match each other.

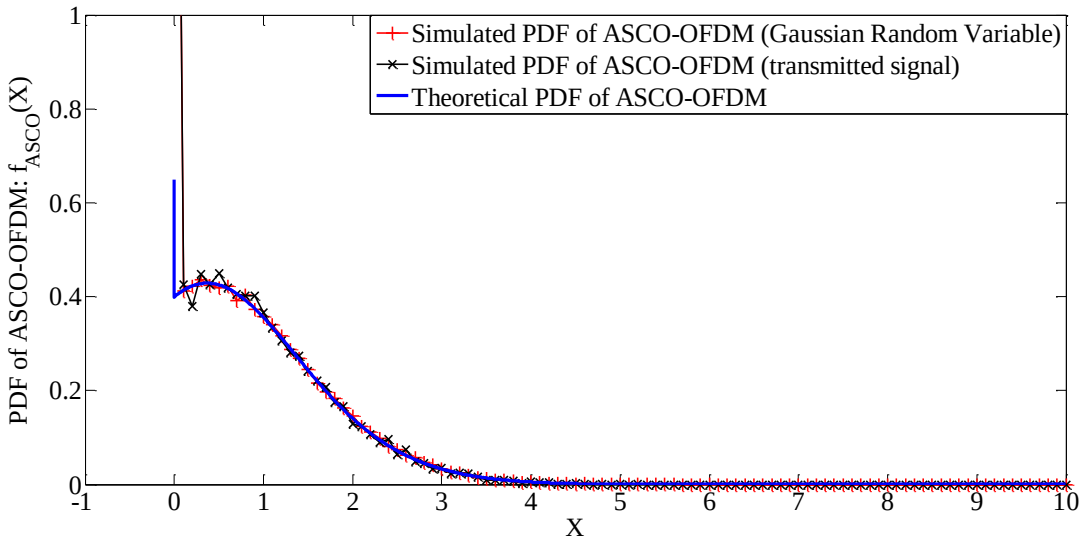

Figure 2.3 Theoretical and Simulated PDF of ASCO-OFDM.

2.3.2 Average Bit Rate/Normalized Bandwidth

For both ADO-OFDM and ASCO-OFDM, $2N-2$ complex symbols are modulated onto the spectrum with length $2N$; hence the normalized bandwidths for both are given by

$N/(N-1)$. In ADO-OFDM, symbols carried on the odd and even subcarriers are drawn from different constellations because odd subcarriers are modulated by ACO-OFDM while even subcarriers are modulated by DCO-OFDM. The average bit rate of ADO-OFDM can be calculated by

$$R_{b,ADO-OFDM} = (\log_2 C_{ACO} + \log_2 C_{DCO})/2 \tag{2.28}$$

where C_{ACO} and C_{DCO} are the constellation sizes of ACO-OFDM symbols and DCO-OFDM symbols, respectively. Therefore, the average bit rate/normalized bandwidth of ADO-OFDM is given by $((\log_2 C_{ACO} + \log_2 C_{DCO})/2)/(N/(N-1))$. In order to improve the power efficiency of ADO-OFDM, DCO-OFDM symbols usually are drawn from small constellations to reduce the DC bias level. For ASCO-OFDM, all information carried in the even subcarriers is separated into two consecutive sub-blocks, x_{ASCO}^{i} and x_{ASCO}^{j}. Thus, half of the information in X_{even} is transmitted by the even components of one sub-block, x_{ASCO}^{i} or x_{ASCO}^{j}. Therefore, the average bit rate of ASCO-OFDM for one sub-block can be obtained by

$$R_{b,ASCO-OFDM} = (\log_2 C_{ACO} + 0.5\log_2 C_{SCO})/2 \tag{2.29}$$

The average bit rate/normalized bandwidth is given by $((\log_2 C_{ACO} + 0.5\log_2 C_{SCO})/2)/(N/(N-1))$, where C_{ACO} and C_{SCO} are similarly defined. By applying different constellations to the odd and even subcarriers of ADO-

OFDM and ASCO-OFDM, the average bit rate/normalized bandwidths for both are compared in Table 2.1.

TABLE 2.1 Average Bit Rate/Normalized Bandwidths of ADO-OFDM and ASCO-OFDM with Different Constellation Combinations

	ADO-OFDM		ASCO-OFDM
ACO-OFDM 4-QAM DCO-OFDM 4-QAM	2	ACO-OFDM 4-QAM SCO-OFDM 4-QAM	1.5
ACO-OFDM 16-QAM DCO-OFDM 4-QAM	3	ACO-OFDM 16-QAM SCO-OFDM 4-QAM	2.5
ACO-OFDM 64-QAM DCO-OFDM 4-QAM	4	ACO-OFDM 64-QAM SCO-OFDM 4-QAM	3.5
ACO-OFDM 16-QAM DCO-OFDM 16-QAM	4	ACO-OFDM 16-QAM SCO-OFDM 16-QAM	3
ACO-OFDM 64-QAM DCO-OFDM 16-QAM	5	ACO-OFDM 64-QAM SCO-OFDM 16-QAM	4
		ACO-OFDM 64-QAM SCO-OFDM 64-QAM	4.5

2.3.3 Optical Power/Bit

In order to find out the accurate optical power per bit, P_{opt}/bit, for both ADO-OFDM and ASCO-OFDM, we sum each value in the transmitted optical signal without adding the cyclic prefix. The total optical power of the transmitted ADO-OFDM signal is computed by

$$P_{opt,ADO} = \sum_{n=0}^{2N-1} x_{ADO}(n) \tag{2.30}$$

The DC bias added in DCO-OFDM comes from Table 2.2. For ASCO-OFDM, the transmitted optical signal has two consecutive sub-blocks, x_{ASCO}^{i} and x_{ASCO}^{j}. Therefore, the total optical power of the transmitted ASCO-OFDM signal is given by

$$P_{opt,ASCO} = \sum_{n=0}^{2N-1} x_{ASCO}^{i}(n) + x_{ASCO}^{j}(n) \tag{2.31}$$

Considering the input of ADO-OFDM, a block of $(N-1)\times 1$ complex symbols is divided into two parts for ACO-OFDM and DCO-OFDM modulation. The $N/2$ complex symbols are modulated onto the odd subcarriers by ACO-OFDM while the $N/2-1$ complex symbols are applied into the even subcarriers for generating DCO-OFDM signals. Therefore, the total transmitted bits for ADO-OFDM are given by

$$T_{b,ADO-OFDM} = (N/2)\log_2 C_{ACO} + (N/2-1)\log_2 C_{DCO} \tag{2.32}$$

For ASCO-OFDM, the input block consisting of $3N/2-1$ complex symbols is separated into three parts. Two blocks of $N/2$ complex symbols are modulated by ACO-OFDM to generate $x_{odd}^{i,c}$ and $x_{odd}^{j,c}$. One block of $N/2-1$ complex symbols is modulated by SCO-OFDM to generate x_{even}^{cn} and x_{even}^{cp}. Therefore, the total transmitted bits for ASCO-OFDM are given by

$$T_{b,ASCO-OFDM} = 2(N/2)\log_2 C_{ACO} + (N/2-1)\log_2 C_{SCO} \quad (2.33)$$

TABLE 2.2 List of ADO-OFDM Constellation Modified from Reference [8] is used in Figures 2.4 and 2.5.

Symbol	ADO-OFDM constellation size	DC bias level
A	ACO-OFDM 4-QAM, DCO-OFDM 4-QAM	5.5dB
B	ACO-OFDM 16-QAM, DCO-OFDM 4-QAM	5.1dB
C	ACO-OFDM 64-QAM, DCO-OFDM 4-QAM	4.3dB
D	ACO-OFDM 16-QAM, DCO-OFDM 16-QAM	7.3dB
E	ACO-OFDM 64-QAM, DCO-OFDM 16-QAM	6.6dB

2.4 Simulation Results

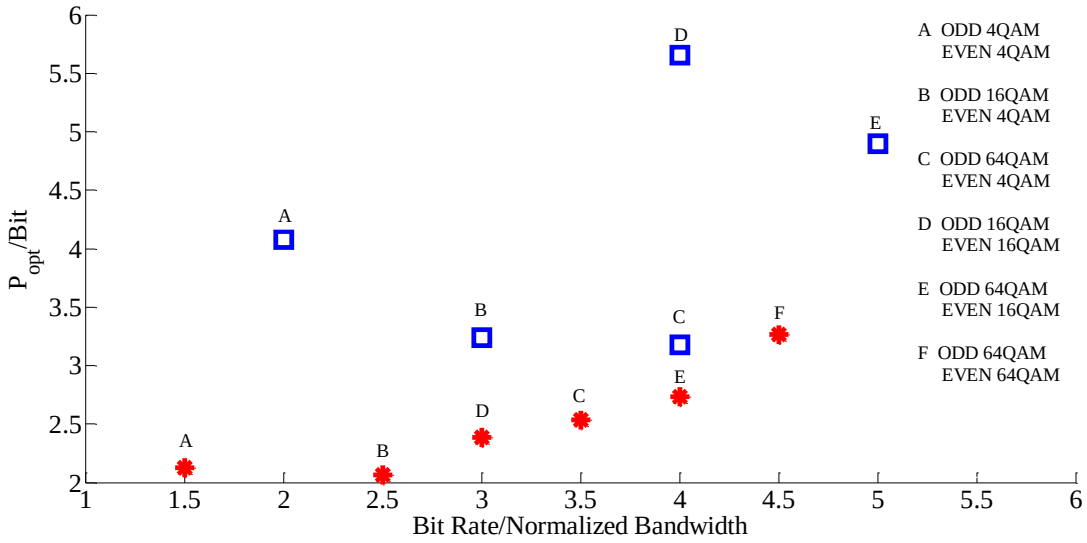

Figure 2.4 Optical Power/Bit versus Bit Rate/Normalized Bandwidth is shown for ADO-OFDM and ASCO-OFDM with different constellation combinations.

The required optical power per bit of ADO-OFDM and ASCO-OFDM is compared in Figure 2.4. Five constellation combinations denoted by A to E, which are listed in Table II, are applied to odd subcarriers (ACO-OFDM) and even subcarriers (DCO- or SCO-OFDM) of two schemes. ADO-OFDM is represented by squares, and ASCO-OFDM is represented by stars. Star F represents ASCO-OFDM with 64-QAM symbols on all subcarriers. If two systems are modulated by the same constellation combination, the bit rate/normalized bandwidth of ASCO-OFDM is less than that of ADO-OFDM. However, ASCO-OFDM requires much less optical power for each bit than ADO-OFDM does due to no DC bias added in the SCO-OFDM modulation. Although the bit rate/normalized bandwidth of ASCO-OFDM is lower, we can use larger constellation combinations to achieve the same bit rate with that of ADO-OFDM. When the same bit rate/normalized bandwidth is achieved, for example square B vs. star D and squares C and D vs. star E, the ASCO-OFDM exhibits more optical power efficiency than ADO-OFDM does. Therefore, ASCO-OFDM is much more optical power efficient compared to ADO-OFDM. Moreover, if the required optical power per bit of ASCO-OFDM is close to that of ADO-OFDM, the bit rate/normalized bandwidth of ASCO-OFDM improves, which is shown as squares B, C vs. star F.

Figure 2.5 shows the SER of ADO-OFDM and ASCO-OFDM applied with different constellation combinations. We use the same marker to represent the same constellation combination. A solid curve represents ASCO-OFDM while a dashed curve represents ADO-OFDM. In the figure, it is obvious that ASCO-OFDM has better SER performance than ADO-OFDM does in the same constellation combination case. Also some specific comparison pairs should be clarified. Comparing the solid circle curve to the dashed plus curve, ASCO-OFDM with 16-4QAM has almost the same SER

performance as 4-4QAM ADO-OFDM, but ASCO-OFDM requires much less optical power and has a higher bit rate as shown in Figure 2.4. When achieving the same bit rate/normalized bandwidth, ASCO-OFDM outperforms ADO-OFDM in terms of the SER performance as well as optical power efficiency, which is shown as a solid square curve (ASCO-OFDM with 16-16) and a dashed circle curve (ADO-OFDM with 16-4). The solid cross curve (ASCO-OFDM with 64-16) and the dashed down-triangle curve (ADO-OFDM with 64-4) have the same performance in terms of SER and bit rate/normalized bandwidth, but the optical power per bit required by ASCO-OFDM is much less than that of ADO-OFDM. Finally, we point out that ASCO-OFDM (solid hexagon) is better than ADO-OFDM (dashed square) in all aspects because it has lower optical power per bit, higher bit rate/normalized bandwidth, and better SER performance.

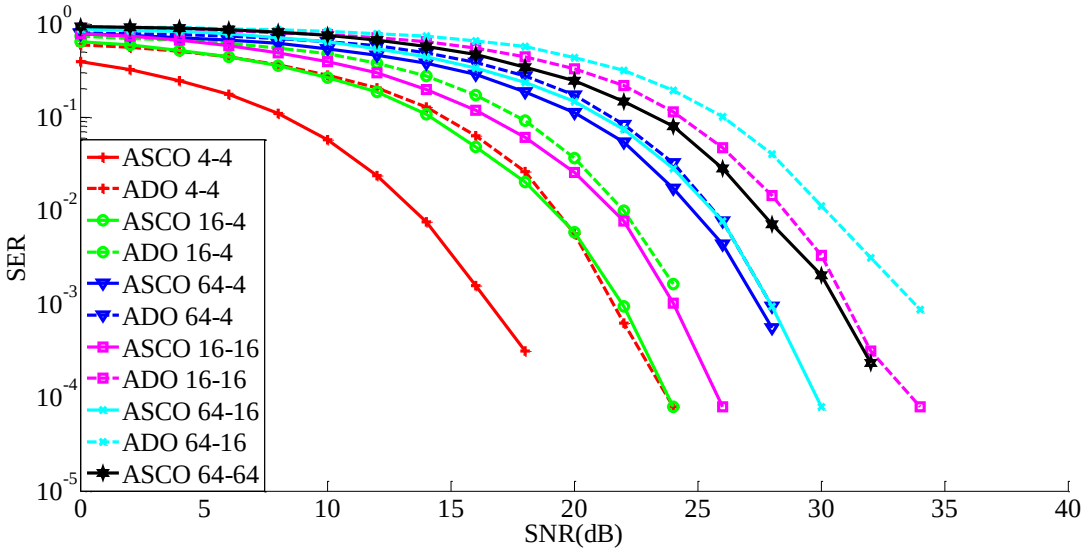

Figure 2.5 Comparison of SER (Symbol Error Rate) versus SNR for ADO-OFDM and ASCO-OFDM with different constellation combinations.

2.5 Conclusion

In this chapter, we proposed a novel OFDM scheme called ASCO-OFDM for IM/DD optical wireless systems. A conventional ACO-OFDM is applied to modulate odd subcarriers and the novel modulation scheme SCO-OFDM is used to modulate even subcarriers. For SCO-OFDM, we successfully adopt two consecutive sub-blocks to transmit the symbols on the even subcarriers without adding DC bias. Since the odd components and the even components of two systems can be separately detected, different constellation combinations are taken into account for modulation. Compared to ADO-OFDM, our novel optical system exhibits better SER performance and requires lower optical power per bit. For these reasons, we believe that ASCO-OFDM is the most attractive choice for IM/DD optical wireless systems.

CHAPTER 3

AN IMPROVED PERFORMANCE RECEIVING TECHNIQUE FOR ASYMMETRICALLY AND SYMMETRICALLY CLIPPING OPTICAL (ASCO)-OFDM

A novel power-efficient optical wireless system, asymmetrically and symmetrically clipping optical (ASCO)-OFDM, has been proposed in Chapter 2. In the ASCO-OFDM modulation scheme, not only odd subcarriers but also even subcarriers can be modulated to transmit clipping optical signals. The odd components of all subcarriers are used to carry ACO-OFDM symbols, and the even components are used to carry SCO-OFDM symbols. Since no DC bias is added to any subcarrier, it makes ASCO-OFDM achieve better performances in terms of optical power and symbol error rate (SER) than ADO-OFDM. Because both the ACO-OFDM and SCO-OFDM clipping noises fall onto the even subcarriers, ACO-OFDM symbols can be directly recovered by extracting the data from the odd subcarriers of received signals. By using the detected ACO-OFDM symbols, we can estimate the ACO-OFDM clipping noise. After removing the ACO-OFDM clipping noise from the even subcarriers, SCO-OFDM symbols can be obtained by a subtraction between two consecutive blocks of SCO-OFDM signals due to the special transmission format.

Conventionally, ACO-OFDM symbols and SCO-OFDM symbols are separately detected at the receiver. However, the SER performance of SCO-OFDM depends on the precision of the estimated ACO-OFDM signals. Therefore, we assume that an improved detection of ACO-OFDM signals can decrease the SER of SCO-OFDM, and it further improves the SER performance of the whole system. In [10], an improved receiving

technique has been proposed to explore the useful information existing in the ACO-OFDM clipping noise. It has been proved that the ACO-OFDM clipping noise is related to the original unclipped signal, and it contains 50% of the transmitted signal power. The improved receiver makes ACO-OFDM achieve up to 3dB better SER performance. In this chapter, we apply this improved ACO-OFDM receiving technique into our ASCO-OFDM receiver to realize the improvement of the whole system [20]. Since a transmitted ASCO-OFDM signal is the sum of an ACO-OFDM signal and a SCO-OFDM signal, the ACO-OFDM clipping cannot be easily obtained from the even subcarriers. We demonstrate how to estimate the ACO-OFDM clipping noise on the even subcarriers.

3.1 An Improved Detector for ACO-OFDM

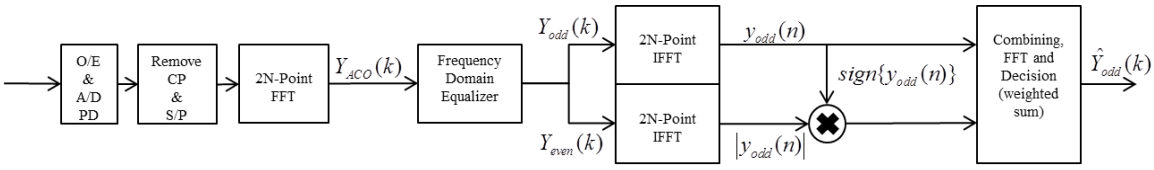

Figure 3.1 Block Diagram of the Improved ACO-OFDM Receiver.

Since the modulation and detection of ACO-OFDM have been introduced in Chapter 1, we directly present the principle of the improved ACO-OFDM detector in this section. A transmitted signal, $X_{ACO}(k)$, is given as follows,

$$X_{ACO}(k) = [0, S_0, 0, S_2 ..., 0, S_{N-2}, 0, S_{N-2}^*, 0, ..., S_2^*, 0, S_0^*]^T \tag{3.1}$$

Supposing the received optical signals are converted into electrical domain and transformed by a 2N-Point FFT to yield $Y_{ACO}(k)$, which is shown as follows:

$$Y_{ACO}(k) = 0.5[C^0, S_0, C^1, S_2, ..., C^{N-2}, S_{N-2}, C^{N-3}, S^*_{N-2}, C^{N-4}, ..., S^*_2, C^{2N-1}, S^*_0]^T \quad (3.2)$$

Compared to $X_{ACO}(k)$, we notice that the amplitude of received signal, $Y_{ACO}(k)$, is half of the original signals due to the clipping approach. Also, some unknown symbols appear on the even subcarriers where should be zeroes, which is shown in the following signal vector,

$$0.5[C^0, 0, C^1, 0..., C^{N-2}, 0, C^{N-3}, 0, C^{N-4}, ..., 0, C^{2N-2}, 0]^T \quad (3.3)$$

It is called ACO-OFDM clipping noise. Fortunately, the transmitted symbols carried on the odd subcarriers are not affected by the ACO-OFDM clipping noise. Thus, the original information can be recovered by only detecting the symbols on the odd subcarriers. However, the ACO-OFDM clipping noise has been proved that it is related to the original symbols in [10]. Here we briefly describe the relation between the original information and the ACO-OFDM clipping noise. The transmitted signals, $x_{ACO}(k)$, can be expressed by a simple mathematics equation,

$$x_{ACO}(n) = 0.5(x_{odd}(n) + |x_{odd}(n)|) \quad (3.4)$$

Note that the original signal with half amplitude is presented by the term, $0.5x_{odd}(n)$. Taken by a FFT, we obtain a Fourier transform pair, which is given by

$$0.5x_{odd}(n) \underset{IFFT}{\overset{FFT}{\rightleftharpoons}} 0.5X_{odd}(k) \tag{3.5}$$

where $0.5X_{odd}(k) = [0, S_0, 0, S_2 ..., 0, S_{N-2}, 0, S_{N-2}^*, 0, ..., S_2^*, 0, S_0^*]^T$. When $0.5|x_{odd}(n)|$ is transformed into the frequency domain, the authors surprisingly found that it was the ACO-OFDM clipping noise that fell onto the even subcarriers, which was given by

$$FFT\{0.5|x_{odd}(n)|\} = 0.5[C^0, 0, C^1, 0..., C^{N-2}, 0, C^{N-3}, 0, C^{N-4}, ..., 0, C^{2N-2}, 0]^T \tag{3.6}$$

Obviously, the time domain form of ACO-OFDM clipping noise is equal to the scaled (0.5) absolute value of original information, $x_{odd}(n)$. Therefore, the equalized received signals will be separated into two parts, $Y_{odd}(k)$ and $Y_{even}(k)$, which are shown as,

$$Y_{odd}(k) = 0.5[0, S_0, 0, S_2, ..., 0, S_{N-2}, 0, S_{N-2}^*, 0, ..., S_2^*, 0, S_0^*]^T \tag{3.7}$$

$$Y_{even}(k) = 0.5[C^0, 0, C^1, 0..., C^{N-2}, 0, C^{N-3}, 0, C^{N-4}, ..., 0, C^{2N-2}, 0]^T \tag{3.8}$$

Then they are transformed back into the time domain to yield two signal vectors, $y_{odd}(n)$ and $|y_{odd}(n)|$. The sign of each element in $y_{odd}(n)$ will be recorded and applied to the corresponding element in $y_{even}(n)$ to yield another estimated signal, which is shown as

$$\bar{y}_{odd}(n) = sign[y_{odd}(n)]|y_{odd}(n)| \tag{3.9}$$

Finally, these two estimated signals are combined with a weighting parameter α to produce an improved output,

$$\hat{Y}_{odd}(k) = \alpha FFT\{y_{odd}(n)\} + (1-\alpha)FFT\{sign[y_{odd}(n)]|y_{odd}(n)|\} \quad (3.10)$$

By using this improved detector (diversity combined receiver), the SER performance improves up to 2.75dB. More details of proof and analysis are demonstrated in [10].

3.2 A Proposed Improved Receiver for ASCO-OFDM

In this section, we present an improved ASCO-OFDM receiver. The block diagram of an improved ASCO-OFDM receiver is shown in Figure 3.2. In the conventional ASCO-OFDM receiver, the odd components, Y_{odd}^{i} and Y_{odd}^{j}, at the output of frequency domain equalizer are directly used to recover X_{odd}^{i} and X_{odd}^{j}. Meanwhile they are used to estimate the ACO-OFDM clipping noise, $\left|X_{odd}^{i}\right|$ and $\left|X_{odd}^{j}\right|$, falling onto the even subcarriers. In the improved ASCO-OFDM receiver, an improved performance block is added into the current receiver to explore the useful information from the even subcarriers of received ASCO-OFDM signals.

The detail of the improved performance block is presented in the shaded area. The input of the block is the equalized received signal vectors, Y^{i} and Y^{j} ($Y^{i,j}$ for short). The other signal vectors are similarly defined. We first separate $Y^{i,j}$ into odd components and

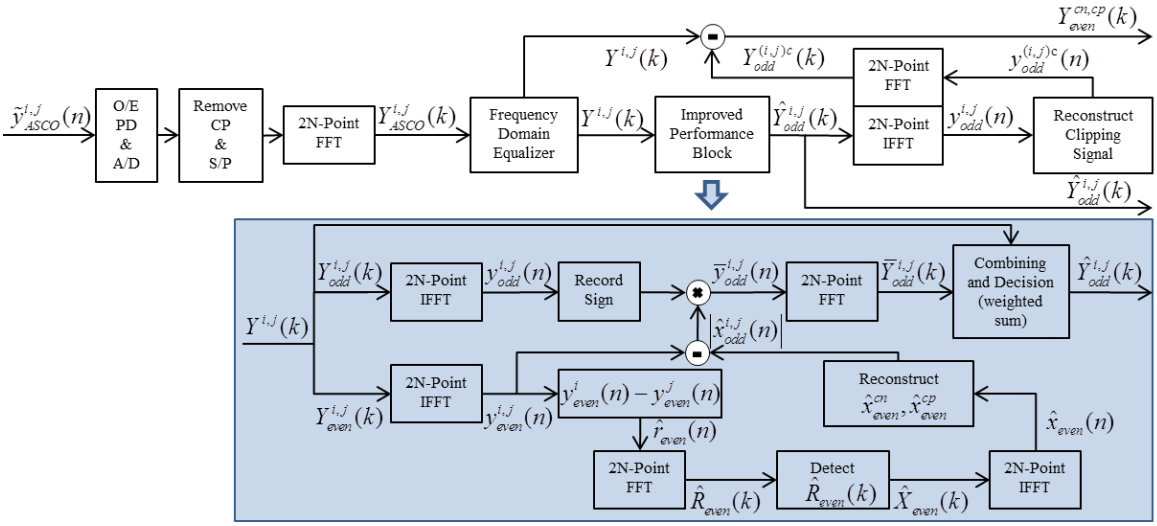

Figure 3.2 Block Diagram of the Improved ASCO-OFDM Receiver (the detail of additional improved performance block is shown in shadowed area).

even components, $Y_{odd}^{i,j}$ and $Y_{even}^{i,j}$. Recall the Equations (2.18) and (2.19), the frequency domain signal vectors, $Y_{odd}^{i,j}$ and $Y_{even}^{i,j}$, are given by

$$Y_{odd}^{i,j} = 0.5X_{odd}^{i,j} + Z_{odd}^{i,j} \tag{3.11}$$

$$Y_{even}^{i} = 0.5(\left|X_{odd}^{i}\right| + X_{even} + \left|X_{even}\right|) + Z_{even}^{i} \tag{3.12}$$

$$Y_{even}^{j} = 0.5(\left|X_{odd}^{j}\right| - X_{even} + \left|X_{even}\right|) + Z_{even}^{j} \tag{3.13}$$

where $Z_{odd}^{i,j}$, Z_{even}^{i}, and Z_{even}^{j} are the FFT of additive white Gaussian noise. $Y_{odd}^{i,j}$ and $Y_{even}^{i,j}$ are taken by a 2N-point IFFT to yield time domain signals $y_{odd}^{i,j}$ and $y_{even}^{i,j}$. Then we record the sign of each value in $y_{odd}^{i,j}$, which is denoted by $sign(y_{odd}^{i,j})$. The time domain signals $y_{even}^{i,j}$ are given by

$$y_{even}^{i} = 0.5\left(\left|x_{odd}^{i}\right| + x_{even} + \left|x_{even}\right|\right) + z_{even}^{i} \tag{3.14}$$

$$y_{even}^{j} = 0.5\left(\left|x_{odd}^{j}\right| - x_{even} + \left|x_{even}\right|\right) + z_{even}^{j} \tag{3.15}$$

From the above equations, we notice that $0.5\left|x_{odd}^{i}\right|$ and $0.5\left|x_{odd}^{j}\right|$ are actually the ACO-OFDM clipping noises. In the improved ACO-OFDM receiver, they can be easily extracted from the even subcarriers. However, the SCO-OFDM signals are transmitted by the even subcarriers in the ASCO-OFDM system. In order to obtain $0.5\left|x_{odd}^{i}\right|$ and $0.5\left|x_{odd}^{j}\right|$ in the even subcarriers, we first make a subtraction between y_{even}^{i} and y_{even}^{j} to yield $\hat{r}_{even}$, which is given by

$$\begin{aligned} \hat{r}_{even} &= y_{even}^{i} - y_{even}^{j} \\ &= 0.5\left(\left|x_{odd}^{i}\right| - \left|x_{odd}^{j}\right|\right) + x_{even} + \left(z_{even}^{i} - z_{even}^{j}\right) \end{aligned} \tag{3.16}$$

$\hat{r}_{even}$ contains the original signal x_{even}, the difference between $0.5\left|x_{odd}^{i}\right|$ and $0.5\left|x_{odd}^{j}\right|$, and the difference between z_{even}^{i} and z_{even}^{j}. We assume that z_{even}^{i} and z_{even}^{j} have the same normal distribution with mean zero and variance σ_z^2. Thus, the difference of z_{even}^{i} and z_{even}^{j} also can be modeled as a normal distribution with mean zero but variance $2\sigma_z^2$. Generally, $x_{odd}^{i,j}$ are modeled as blocks of Gaussian random variables with mean zero and variance σ^2. Then the absolute version of $x_{odd}^{i,j}$ follows a half-normal distribution [21], which is given by

$$f(x;\sigma)=\frac{\sqrt{2}}{\sigma\sqrt{\pi}}\exp(-\frac{x^2}{2\sigma^2}) \quad x\in\left|x_{odd}^{i,j}\right| \tag{3.17}$$

where the mean and variance of the half-normal distribution are $\frac{\sigma\sqrt{2}}{\sqrt{\pi}}$ and $\sigma^2(1-\frac{2}{\pi})$, respectively. $\left|x_{odd}^{i}\right|$ and $\left|x_{odd}^{j}\right|$ are independent, therefore the distribution of the difference is the convolution of the distributions, $f(y)=f(x_1)\otimes f(x_2)$. The PDF of $\left|x_{odd}^{i}\right|-\left|x_{odd}^{j}\right|$ is given by

$$f(y)=\frac{1}{\sigma\sqrt{\pi}}\exp(-\frac{y^2}{4\sigma^2}) \tag{3.18}$$

The PDF is derived in Appendix D. Thus, we assume that the original signal x_{even} is distorted by another white Gaussian noise with mean zero and variance $\frac{\sigma^2}{2}(1-\frac{2}{\pi})$ (due to the scalar 0.5). $\hat{r}_{even}$ is taken by a 2N-point FFT to yield $\hat{R}_{even}$ for detection. Then the estimated symbols, $\hat{X}_{even}$, are transformed into the time domain to produce $\hat{x}_{even}$. In the following block, we reconstruct two reference clipping signals, $\hat{x}_{even}^{cn}$ and $\hat{x}_{even}^{cp}$, which are given by

$$\hat{x}_{even}^{cn}=0.5(\hat{x}_{even}+\left|\hat{x}_{even}\right|) \tag{3.19}$$

$$\hat{x}_{even}^{cp}=0.5(-\hat{x}_{even}+\left|\hat{x}_{even}\right|) \tag{3.20}$$

Subtracting these two reference clipping signals, $\hat{x}_{even}^{cn}$ and $\hat{x}_{even}^{cp}$, from y_{even}^{i} and y_{even}^{j}, respectively, we obtain the estimated $\left|\hat{x}_{odd}^{i}\right|$ and $\left|\hat{x}_{odd}^{j}\right|$ plus their corresponding noises, which are given by

$$y_{even}^{i} - \hat{x}_{even}^{cn} = 0.5\left|\hat{x}_{odd}^{i}\right| + z_{even}^{i} \tag{3.21}$$

$$y_{even}^{j} - \hat{x}_{even}^{cp} = 0.5\left|\hat{x}_{odd}^{j}\right| + z_{even}^{j} \tag{3.22}$$

Then the estimated signals $\left|\hat{x}_{odd}^{i}\right|$ and $\left|\hat{x}_{odd}^{j}\right|$ are multiplied by the sign of x_{odd}^{i} and x_{odd}^{j}, respectively to yield $\bar{y}_{odd}^{i}$ and $\bar{y}_{odd}^{j}$. They are taken by a 2N-point FFT to yield another two frequency domain reference signal vectors, $\bar{Y}_{odd}^{i}$ and $\bar{Y}_{odd}^{j}$. We combine these two reference signal vectors with the odd components, Y_{odd}^{i} and Y_{odd}^{j}, to obtain an improved estimate by a weighted sum

$$\hat{Y}_{odd}^{i} = \alpha Y_{odd}^{i} + (1-\alpha)\bar{Y}_{odd}^{i} \tag{3.23}$$

$$\hat{Y}_{odd}^{j} = \alpha Y_{odd}^{j} + (1-\alpha)\bar{Y}_{odd}^{j} \tag{3.24}$$

α is defined as the ratio between the SNR of $Y_{odd}^{i,j}$ and SNR of $\bar{Y}_{odd}^{i,j}$. The subsequent operations are the same as those in the conventional ASCO-OFDM receiver. We can use the output of the improved performance block, $\hat{Y}_{odd}^{i}$ and $\hat{Y}_{odd}^{j}$, to recover the odd components of received signals. Then $Y_{odd}^{i,c}$ and $Y_{odd}^{j,c}$ can be reconstructed and are

subtracted from Y^i and Y^j to yield Y_{even}^{cn} and Y_{even}^{cp}. Finally, we obtain the even components of received signals by applying a form that $X_{even} = Y_{even}^{cn} - Y_{even}^{cp}$.

3.3 Analysis and Simulation Results

In this section, we present the simulation results for a conventional receiver and an improved receiver of ASCO-OFDM. In order to apply a 2N-point FFT/IFFT, we set N=64, and thus each input block has 3N/2-1 independent complex symbols, which can be drawn from 4-QAM, 16-QAM, or 64-QAM. Because the odd subcarriers and the even subcarriers are separately modulated, different constellation combinations are taken into account for comparison. The average power of each symbol drawn from different constellations is normalized. Thus, each blocks, such as x_{odd}^i, x_{odd}^j and x_{even}, have the same variance σ^2. Three combining methods, Equal Gain Combining (EGC), Fixed Gain Combining (FGC), and Maximal Ratio Combining (MRC) are considered for the improved ASCO-OFDM receiver with different values α in Equations (3.23), (3.24). Since $\left|\hat{x}_{odd}^i\right|$ and $\left|\hat{x}_{odd}^j\right|$ are obtained by subtracting the estimated symbols $\hat{X}_{even}$ and are distorted by other noises, the weighting coefficient (1-α) of the second reference signals, $\bar{Y}_{odd}^i$ and $\bar{Y}_{odd}^j$, should be less than 0.5. Thus, EGC should not be applied in the improved receiver. The detection of $\hat{X}_{even}$ gets harder as the constellation size increases. Without considering the noise power, σ_Z^2, in Equation (3.16), the power of x_{even} and $0.5(\left|x_{odd}^i\right| - \left|x_{odd}^j\right|)$ are σ^2 and $\frac{\sigma^2}{2}(1-\frac{2}{\pi})$, respectively, which is almost 7.4dB between them. If each sample in x_{even} is converted from 4-QAM symbols, it can be correctly

detected when SNR is around 7.4dB. However, if each sample in x_{even} is converted from 16-QAM and 64-QAM, the detected signals still have high symbol error rate around 7.4dB SNR case. The improvement is negligible when the data on the even subcarriers are drawn from 16-QAM or 64-QAM. Therefore, only 4-QAM can be applied to the even subcarriers but there is no limitation on the constellation for the odd subcarriers.

Because we have the PDF of each term in Equations (2.12) and (2.13), we can calculate the signal power of each term as well as the transmitted signals, x^i_{ASCO} and x^j_{ASCO}. Moreover, we found that the variance of transmitted signal is the sum of variance of each term, for example

$$\mathrm{var}(x^i_{ASCO}) = 0.25[\mathrm{var}(x^i_{odd}) + \mathrm{var}(|x^i_{odd}|) + \mathrm{var}(x_{even}) + \mathrm{var}(|x_{even}|)] \qquad (3.25)$$

Thus, we can use algebraic calculation to obtain the weighting coefficient α for MRC. If 4-QAM is applied to the odd subcarriers, the weighting coefficient α is approximately equal to 0.7. Through algebraic calculation, the weighting coefficients are $\alpha \approx 0.867$ for 16-QAM and $\alpha \approx 0.935$ for 64-QAM. The optimal values have not been studied further for different constellations, but they are close to these given values. In the simulation, we present the SER performance of FGC with the values of $\alpha = 0.7$ for 4-4QAM, $\alpha = 0.85$ for 16-4QAM, and $\alpha = 0.9$ for 64-4QAM.

The SER performance of improved ASCO-OFDM receiver is shown in Figure 3.3. We use the same marker to represent the same constellation combination. A solid curve represents an improved receiver while a dashed curve represents a conventional receiver. The improved receiver achieves different improvement under different

constellation combination cases. Compared to a conventional receiver (dashed circle curve), the SER performance of an improved receiver (solid circle curve) obtains almost 1.5dB gain when all subcarriers are modulated by 4-QAM. When the odd subcarriers are used to carry 16-QAM symbols, the improved receiver (solid square curve) outperforms a conventional receiver (dashed square curve) with 1dB gain. When 64-QAM is applied to the odd subcarriers, the improve receiver (solid cross curve) achieves 0.5dB gain.

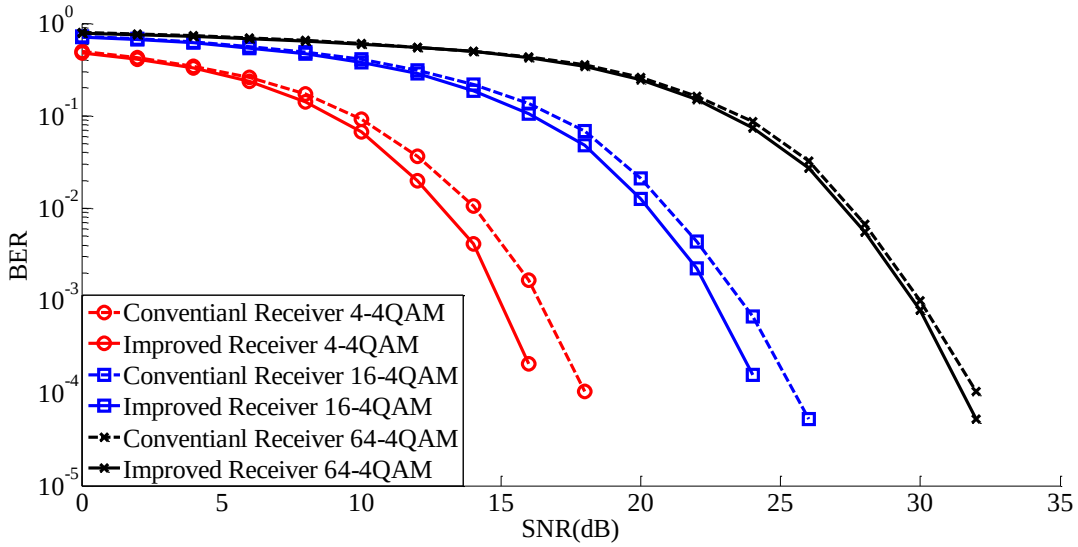

Figure 3.3 Comparison of SER (Symbol Error Rate) versus SNR for ASCO-OFDM and improved ASCO-OFDM with different constellation combinations.

3.4 Conclusion

In the conventional ASCO-OFDM receiver, ACO-OFDM signals are directly detected on the odd subcarriers, and then SCO-OFDM signals can be obtained by subtracting the absolute version of ACO-OFDM signals from even subcarriers. So the detection of SCO-OFDM depends on the detected ACO-OFDM signals. An improved decoding technique for ACO-OFDM signals has been introduced in [10]. Based on this idea, we applied this technique into ASCO-OFDM receiver to improve the symbol error rate (SER)

performance of ACO-OFDM signals. Thus, we assume that the SER of SCO-OFDM signals will be reduced as well. All the operations are presented in the improved performance block and it can be easily added into a conventional ASCO-OFDM receiver without any change to the other part of the whole system.

CHAPTER 4

INFORMATION RATES OF ASCO-OFDM AND ADO-OFDM

Channel capacity is an important benchmark for designing a communication system. Since OWC is an attractive alternative to RFC for the use of indoor high speed data transmission, the performances of IM/DD optical wireless systems have received more attention, especially the channel capacity. Because information data streams are transmitted by visible light, the emitted optical power has to be subject to an average power constraint. In the Shannon capacity formula, the maximum entropy with an average power constraint is achieved by Gaussian distribution. But if the input signal is unipolar, the maximum entropy is given by exponential distribution in [22]. Thus, the Shannon capacity formula derived for bipolar signals cannot be used in IM/DD OWCs. As a result, the upper and lower bounds for particular cases have been studied by many researchers. You and Kahn derived the upper bound for an IM/DD optical system with multiple subcarrier modulation by using sphere packing techniques [23]. Farid and Hranilovic utilized signal space geometry and a sphere packing argument to derive a tighter upper bound on the capacity of optical wireless IM/DD channels with pulse amplitude modulation (PAM) signals [24]. The lower bound can be easily obtained by calculating the mutual information of any input distribution satisfying non-negativity and average optical power constraint. In [24], Farid and Hranilovic applied this approach to obtain a tight lower bound at both low and high SNRs for a family of discrete distributions. Moreover, the information rate of a particular system can be numerically computed when the corresponding input source distribution is known. In [19], Li, Mardling and Armstrong compared the information rates of transmitted signal samples

having either clipped Gaussian or exponential distribution where transmitted signals are subject to an average optical power constraint.

In this chapter, the information rates of ASCO-OFDM and ADO-OFDM are investigated [25]. By using the derived PDF of ADO-OFDM in [8], the information rate of ADO-OFDM is numerically calculated. The odd component of transmitted ASCO-OFDM signals (ACO-OFDM signals) follows a clipped Gaussian distribution in [18-19]. We assume that the even component of ASCO-OFDM signals (SCO-OFDM signals) follows a clipped Gaussian distribution as well because it is generated in the same way as the ACO-OFDM signals. Thus, the PDF of an ASCO-OFDM signal is the convolution of two clipped Gaussian distributions. The PDF of transmitted ASCO-OFDM signals presented in [9] is a special case because we assume the deviation of ACO-OFDM signals is equal to that of SCO-OFDM signals. In order to obtain the information rates of ASCO-OFDM for different cases, a general PDF solution is derived.

4.1 Probability Density Function of ADO-OFDM Signals

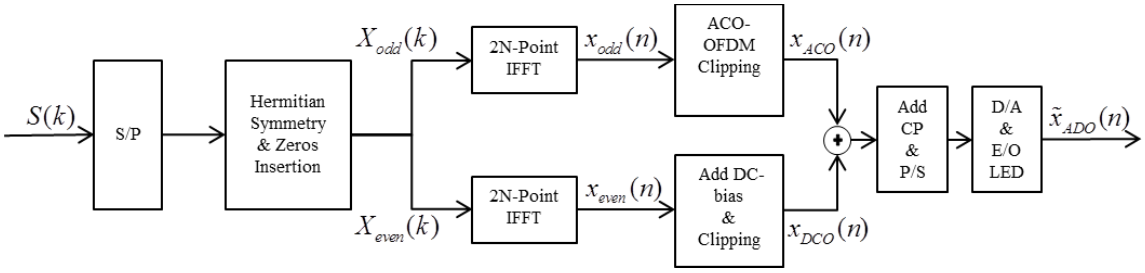

Figure 4.1 Transmitter Structure of ADO-OFDM.

Figure 4.1 shows the structure of ADO-OFDM transmitter. A block of $(N-1)\times 1$ complex data symbols $S=[S_0, S_1, ..., S_{N-2}]^T$ is input to the ADO-OFDM system where the symbols are drawn from constellations such as 4-QAM, 16-QAM, or 64-QAM. In order

to obtain a real signal, this block of complex data symbols is combined with its conjugate sequence $S^* = [S_0^*, S_1^*, ..., S_{N-2}^*]^T$ in reverse order to form a $2(N-1)\times 1$signal vector that has Hermitian symmetry as follows, $[S_0, S_1, ..., S_{N-2}, S_{N-2}^*, ..., S_1^*, S_0^*]^T$. Two zeroes are respectively inserted at the first and at the middle of this signal vector, which is shown as $X = [0, S_0, S_1, ..., S_{N-2}, 0, S_{N-2}^*, ..., S_1^*, S_0^*]^T$. Then X is divided into two $2N\times 1$ signal vectors, X_{odd} and X_{even}, that consist of odd components and even components of X, where $X_{odd} = [0, S_0, 0, S_2 ..., 0, S_{N-2}, 0, S_{N-2}^*, 0, ..., S_2^*, 0, S_0^*]^T$ and $X_{even} = [0, 0, S_1, 0, S_3 ..., S_{N-3}, 0, 0, 0, S_{N-3}^*, ..., S_3^*, 0, S_1^*, 0]^T$. Both X_{odd} and X_{even} are converted by a 2N-point IFFT to yield two real bipolar signal vectors, x_{odd} and x_{even}, respectively. Generally, the output of IFFT, x_{odd} and x_{even}, can be modeled as a block of Gaussian random variables with mean zero and variance $\sigma_A^2 = E\{x_{odd}^2\}$ and $\sigma_D^2 = E\{x_{even}^2\}$, respectively. In an ACO-OFDM clipping block, the negative values in x_{odd} are clipped to zero to produce a signal, x_{ACO}, consisting of non-negative values. Thus, x_{ACO} follows a clipped Gaussian distribution [18-19], which is given by

$$f_{ACO}(a) = \frac{1}{\sqrt{2\pi}\sigma_A} \exp(\frac{-a^2}{2\sigma_A^2}) u(a) + \frac{1}{2}\delta(a) \tag{4.1}$$

Another signal, x_{DCO}, is obtained by adding a DC bias to x_{even} and setting the remaining negative values to zero. In order to avoid the DCO-OFDM clipping noise, a large DC-bias should be added which makes the transmitted optical signal inefficient in terms of optical power. Thus, the performance of DCO-OFDM depends on the DC bias

level. The DC bias is denoted by B_{DC} , which can be defined as the following: $B_{DC} = \mu\sqrt{E\{x_{even}^2\}}$. $10\log_{10}(\mu^2+1)dB$ is the decibel form of B_{DC} , where μ is a proportionality constant. The PDF of x_{DCO} is given by [2, 18]

$$f_{DCO}(b) = \frac{1}{\sqrt{2\pi}\sigma_D}\exp(\frac{-(b-B_{DC})^2}{2\sigma_D^2})u(b) + Q(\frac{B_{DC}}{\sigma_D})\delta(b) \tag{4.2}$$

where $u(x)$ is a unit step function and $\delta(x)$ is the Dirac delta function. Because the transmitted signal x_{ADO} is the sum of x_{ACO} and x_{DCO} , the distribution of x_{ADO} is the convolution of the PDFs of x_{ACO} and x_{DCO} , which is given by [8],

$$\begin{aligned} f_{ADO}(z) = {} & \frac{1}{\sqrt{2\pi(\sigma_A^2+\sigma_D^2)}}\exp(\frac{-(z-B_{DC})^2}{2(\sigma_A^2+\sigma_D^2)})[Q(\frac{z\sigma_D^2+B_{DC}\sigma_A^2}{-\sqrt{\sigma_D^2\sigma_A^2(\sigma_A^2+\sigma_D^2)}}) - Q(\frac{z\sigma_A^2-B_{DC}\sigma_A^2}{\sqrt{\sigma_D^2\sigma_A^2(\sigma_A^2+\sigma_D^2)}})] \\ & +[\frac{1}{\sqrt{2\pi}\sigma_A}\exp(\frac{-z^2}{2\sigma_A^2})Q(\frac{B_{DC}}{\sigma_D}) + \frac{1}{2\sqrt{2\pi}\sigma_D}\exp(\frac{-(z-B_{DC})^2}{2\sigma_D^2})]u(z) + \frac{1}{2}\delta(z)Q(\frac{B_{DC}}{\sigma_D}) \end{aligned} \tag{4.3}$$

4.2 Probability Density Function of ASCO-OFDM Signals

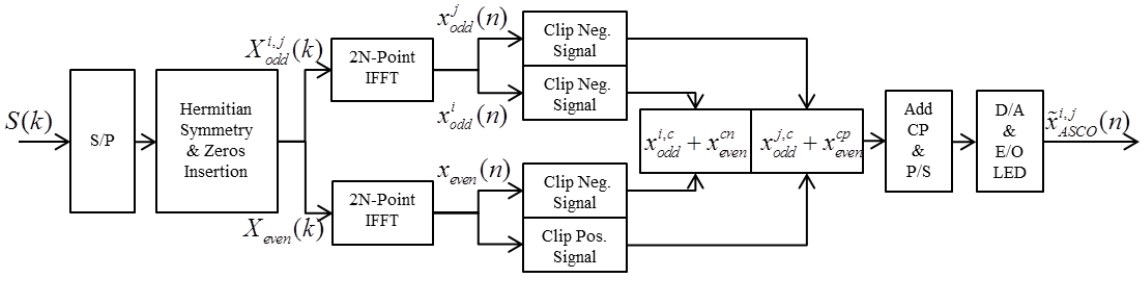

Figure 4.2 Transmitter Structure of ASCO-OFDM.

The transmitter structure of ASCO-OFDM has been shown in Figure 4.2. The input of the ASCO-OFDM system is a block of $(3N/2-1)\times 1$ complex data symbols $S=[S_0,S_1,...,S_{N-2}]^T$ mapped from constellations such as 4-QAM, 16-QAM, or 64-QAM. The input block is then separated into three parts, which have two $(N/2)\times 1$ signal vectors and one $(N/2-1)\times 1$ signal vector. In order to obtain a real signal, we have to make the input have Hermitian symmetry. Two $(N/2)\times 1$ signal vectors are respectively combined with their conjugate sequences and are inserted by zeroes into the even subcarriers to form two $2N\times 1$ signal vectors, X_{odd}^{i} and X_{odd}^{j}, which are given by $X_{odd}^{i}=[0,S_0^i,0,S_1^i...,0,S_{N/2}^i,0,S_{N/2}^{i*},0,...,S_1^{i*},0,S_0^{i*}]^T$ and $X_{odd}^{j}=[0,S_0^j,0,S_1^j...,0,S_{N/2}^j,0,S_{N/2}^{j*},0,...,S_1^{j*},0,S_0^{j*}]^T$. The $(N/2-1)\times 1$ signal vector is defined in a similar way with zeroes inserted into the odd subcarriers to form a $2N\times 1$ signal vector X_{even} as follows $X_{even}=[0,0,S_0,0,S_1...,S_{N/2-1},0,0,0,S_{N/2-1}^*,...,S_1^*,0,S_0^*,0]^T$. All three signal vectors X_{odd}^{i}, X_{odd}^{j} and X_{even} are constrained to Hermitian symmetry. They are taken by a 2N-point IFFT to produce real bipolar signal vectors x_{odd}^{i}, x_{odd}^{j} and x_{even}, respectively. To ensure the non-negative requirement of transmitted signals, all negative values in x_{odd}^{i} and x_{odd}^{j} are clipped to zero to generate $x_{odd}^{i,c}$ and $x_{odd}^{j,c}$. As each sample in x_{even} is converted from even subcarriers, it has the relation that $x_{even}(n)=x_{even}(n+N)$, which is proved in [9]. By clipping the negative values, half of the information carried in x_{even} is lost. Thus two signal vectors, x_{even}^{cn} and x_{even}^{cp}, are generated for transmitting the information in x_{even}. x_{even}^{cn} represents that all negative values of x_{even} are clipped to zero. x_{even}^{cp} represents that all positive values of x_{even} are clipped to zero and the negative values

are turned to positive. Then we construct the transmitted signal that consist of two consecutive sub-blocks, x_{ASCO}^{i} and x_{ASCO}^{j}, which are given by

$$x_{ASCO}^{i} = x_{odd}^{i,c} + x_{even}^{cn} \tag{4.4}$$

$$x_{ASCO}^{j} = x_{odd}^{j,c} + x_{even}^{cp} \tag{4.5}$$

Note that $x_{odd}^{i,c}$, $x_{odd}^{j,c}$, x_{even}^{cn} and x_{even}^{cp} are all real and non-negative signals. The PDFs of $x_{odd}^{i,c}$ and x_{even}^{cn} are respectively given by

$$f_{x_{odd}^{i,c}}(\alpha) = \frac{1}{\sqrt{2\pi}\sigma_A} e^{-\frac{\alpha^2}{2\sigma_A^2}} u(\alpha) + \frac{1}{2}\delta(\alpha) \tag{4.6}$$

$$f_{x_{even}^{cn}}(\beta) = \frac{1}{\sqrt{2\pi}\sigma_S} e^{-\frac{\beta^2}{2\sigma_S^2}} u(\beta) + \frac{1}{2}\delta(\beta) \tag{4.7}$$

Although $x_{odd}^{i,c}$ and x_{even}^{cn} have the same distribution, $x_{odd}^{i,c}$ is an ACO-OFDM signal and x_{even}^{cn} is a SCO-OFDM signal. We use σ_A and σ_S to distinguish them where σ_A and σ_S are the standard deviation of the unclipped signal, such as x_{odd}^{i} (x_{odd}^{j}) and x_{even}. When $\sigma_A = \sigma_S$, the PDF of x_{ASCO}^{i} is presented in [9]. Since $x_{odd}^{i,c}$ and x_{even}^{cn} are separately modulated and generated, the variance of $x_{odd}^{i}(x_{odd}^{j})$ and x_{even} can be different, which means σ_A is not always equal to σ_S. Then, we derive the general PDF of x_{ASCO}^{i} in this

section. We know $x_{ASCO}^{i} = x_{odd}^{i,c} + x_{even}^{cn}$, so the general PDF of x_{ASCO}^{i} is derived by convoluting $f_{x_{odd}^{i,c}}(\alpha)$ and $f_{x_{even}^{cn}}(\beta)$,

$$f(\chi) = \int_{-\infty}^{\infty} f_{x_{odd}^{i,c}}(\alpha) f_{x_{even}^{cn}}(\chi - \alpha) d\chi \tag{4.8}$$

Substituting Equations (4.6) and (4.7) into Equation (4.8), we obtain the general PDF of x_{ASCO}^{i},

$$\begin{aligned} f_{x_{ASCO}^{i}}(\chi) = & \frac{1}{2\sqrt{2\pi(\sigma_A^2 + \sigma_S^2)}} \exp\left(\frac{-\chi^2}{2(\sigma_A^2 + \sigma_S^2)}\right)\left[erf\left(\frac{\sigma_A \chi}{\sigma_S \sqrt{2(\sigma_A^2 + \sigma_S^2)}}\right) + erf\left(\frac{\sigma_S \chi}{\sigma_A \sqrt{2(\sigma_A^2 + \sigma_S^2)}}\right)\right] \\ & + \left[\frac{1}{2\sqrt{2\pi\sigma_A^2}} \exp\left(\frac{-\chi^2}{2\sigma_A^2}\right) + \frac{1}{2\sqrt{2\pi\sigma_S^2}} \exp\left(\frac{-\chi^2}{2\sigma_S^2}\right)\right] u(\chi) + \frac{1}{4}\delta(\chi) \end{aligned} \tag{4.9}$$

where $erf(x)$ is the error function. The mean and variance of x_{ASCO}^{i} are $(\sigma_A + \sigma_S)/\sqrt{2\pi}$ and $(\pi - 1)(\sigma_A^2 + \sigma_S^2)/2\pi$, respectively.

4.3 Information Rates of ADO-OFDM and ASCO-OFDM

Channel capacity can be obtained by calculating the maximum mutual information between input and output of the channel, where the maximization is subject to the input distribution. The information rate of a particular optical system can be obtained in the same approach when the input distribution is limited to a certain power level. In optical wireless communications, the information is modulated into the intensity of optical

carriers, which means the variables in the input distribution must be real and non-negative. Moreover, the average optical power of the transmitted signal must be limited due to the eye safety regulations. Thus, a distribution satisfying the requirements, real, non-negative, and optical power constraint, results in the information rate of an optical wireless IM/DD system. Then we numerically calculate the information rates of ASCO-OFDM and ADO-OFDM.

We first present the steps of calculating the channel capacity. If the transmitted optical signal is $x(n)$ and the optical channel is $h(n)$, the arrival signal is given by $y(n) = x(n) * h(n) + w(n)$. The optical channel is considered as a flat channel; thus we assume $h(n) = 1$. The combination of all noise $w(n)$ is approximately modeled as additive white Gaussian noise. Note that the cyclic prefix is not considered. Then the channel capacity is given by

$$C = \max I(x, y) \tag{4.10}$$

where $I(x, y)$ is the mutual information, which is given by

$$\begin{aligned} I(x, y) &= h(y) - h(w) \\ &= -\int_{-\infty}^{\infty} f(y) \log_2 f(y) dy - 0.5 \log_2 2\pi 2\sigma_n^2 \end{aligned} \tag{4.11}$$

$h(y)$ and $h(w)$ are the differential entropy of received signals and Gaussian noise, respectively. $f(y)$ is the distribution of transmitted signals plus noise.

4.3.1 The PDF of Transmitted ADO-OFDM Signals Plus Noise

The ADO-OFDM transmitted signals pass through optical channel to yield,

$$y_{ADO}(n) = x_{ADO}(n) + w(n) \tag{4.12}$$

The distribution of y_{ADO} is the convolution of the PDF of x_{ADO} and the Gaussian distribution,

$$\begin{aligned} f_{y_{ADO}}(y) &= \int_{-\infty}^{\infty} f_{x_{ADO}}(z) f_n(y-z)dz \\ &= \frac{1}{2\pi\sigma_n\sqrt{\sigma_A^2+\sigma_D^2}} \int_0^{\infty} \exp\left(\frac{-(x-B_{DC})^2}{2(\sigma_A^2+\sigma_D^2)}\right) \exp\left(\frac{-(y-x)^2}{2\sigma_n^2}\right) \\ &\bullet\left[Q\left(\frac{x\sigma_D^2+B_{DC}\sigma_A^2}{-\sqrt{\sigma_D^2\sigma_A^2(\sigma_A^2+\sigma_D^2)}}\right) - Q\left(\frac{x\sigma_A^2-B_{DC}\sigma_A^2}{\sqrt{\sigma_D^2\sigma_A^2(\sigma_A^2+\sigma_D^2)}}\right)\right]dx \\ &+ \frac{1}{2\sqrt{2\pi(\sigma_A^2+\sigma_n^2)}} Q\left(\frac{B_{DC}}{\sigma_D}\right) \exp\left(\frac{-y^2}{2(\sigma_A^2+\sigma_n^2)}\right)\left[erfc\left(\frac{-y\sigma_A}{\sigma_n\sqrt{2(\sigma_A^2+\sigma_n^2)}}\right)\right] \\ &+ \frac{1}{4\sqrt{2\pi(\sigma_D^2+\sigma_n^2)}} \exp\left(\frac{-(y-B_{DC})^2}{2(\sigma_D^2+\sigma_n^2)}\right)\left[erfc\left(\frac{-(B_{DC}\sigma_n^2+y\sigma_D^2)}{\sigma_D\sigma_n\sqrt{2(\sigma_D^2+\sigma_n^2)}}\right)\right] \\ &+ \frac{1}{2\sqrt{2\pi\sigma_n^2}} Q\left(\frac{B_{DC}}{\sigma_D}\right) \exp\left(\frac{-y^2}{2\sigma_n^2}\right) \end{aligned} \tag{4.13}$$

4.3.2 The PDF of Transmitted ASCO-OFDM Signals Plus Noise

The ASCO-OFDM transmitted signal has two consecutive sub-blocks, y_{ASCO}^i and y_{ASCO}^j. Here we consider the first sub-block y_{ASCO}^i, which is given by

$$y_{ASCO}^i(n) = x_{ASCO}^i(n) + w^i(n) \tag{4.14}$$

To calculate the information rate of ASCO-OFDM, we derive the distribution of y_{ASCO}^{i} by convoluting the PDF of x_{ASCO}^{i} and the Gaussian distribution,

$$
\begin{aligned}
f_{y_{ASCO}^{i}}(y) &= \int_{-\infty}^{\infty} f_{x_{ASCO}^{i}}(\chi) f_n(y-\chi) d\chi \\
&= \frac{\sqrt{2}}{4\pi\sqrt{\sigma_A^2+\sigma_S^2+\sigma_n^2}} \exp\left(\frac{-y^2}{2(\sigma_A^2+\sigma_S^2+\sigma_n^2)}\right) \int_{\frac{-y\sqrt{\sigma_A^2+\sigma_S^2}}{\sigma_n\sqrt{2(\sigma_A^2+\sigma_S^2+\sigma_n^2)}}}^{\infty} \exp(-m^2) \\
&\bullet\left[erf\left(\frac{\sigma_A\sigma_n m}{\sigma_S\sqrt{\sigma_A^2+\sigma_S^2+\sigma_n^2}} + \frac{y\sigma_A\sqrt{2(\sigma_A^2+\sigma_S^2)}}{2\sigma_S(\sigma_A^2+\sigma_S^2+\sigma_n^2)}\right)\right. \\
&\left. + erf\left(\frac{\sigma_S\sigma_n m}{\sigma_A\sqrt{\sigma_A^2+\sigma_S^2+\sigma_n^2}} + \frac{y\sigma_S\sqrt{2(\sigma_A^2+\sigma_S^2)}}{2\sigma_A(\sigma_A^2+\sigma_S^2+\sigma_n^2)}\right)\right] dm \\
&+ \frac{1}{4\sqrt{2\pi(\sigma_A^2+\sigma_n^2)}} \exp\left(\frac{-y^2}{2(\sigma_A^2+\sigma_n^2)}\right)\left[erfc\left(\frac{-y\sigma_A}{\sigma_n\sqrt{2(\sigma_A^2+\sigma_n^2)}}\right)\right] \\
&+ \frac{1}{4\sqrt{2\pi(\sigma_S^2+\sigma_n^2)}} \exp\left(\frac{-y^2}{2(\sigma_S^2+\sigma_n^2)}\right)\left[erfc\left(\frac{-y\sigma_S}{\sigma_n\sqrt{2(\sigma_S^2+\sigma_n^2)}}\right)\right] \\
&+ \frac{1}{4\sqrt{2\pi\sigma_n^2}} \exp\left(\frac{-y^2}{2\sigma_n^2}\right)
\end{aligned}
\tag{4.15}
$$

Substituting Equations (4.13), (4.15) into Equation (4.11), the information rates of ADO-OFDM and ASCO-OFDM can be respectively obtained for different SNRs. The results are presented in Figure 4.7.

4.4 Simulation Results

In this section, we first present the cumulative distribution function (CDF) curves and probability density function (PDF) curves for the transmitted and received signals of ADO-OFDM and ASCO-OFDM, respectively. In Figures 4.3, 4.4, 4.5 and 4.6, red curve represents the theoretical result of transmitted signals. The other curves, blue, green, and

black, are used to display the results of received signals in different SNRs. The average optical power is defined as the mean of transmitted optical signals, which is given by $P_{opt,x} = E\{x(n)\}$. Without loss of generality, we set the average optical power to 1, i.e. $(\sigma_A + \sigma_S)/\sqrt{2\pi} = 1$. The mean of ADO-OFDM transmitted signals is presented in [8] and it has no closed form, but we still can make the transmitted signals achieve the average power constraint by simulating the values of σ_A and σ_D. The CDF curves of ADO-OFDM are presented in Figure 4.3. Obviously, the horizontal ordinate of crossover point is equal to 1.

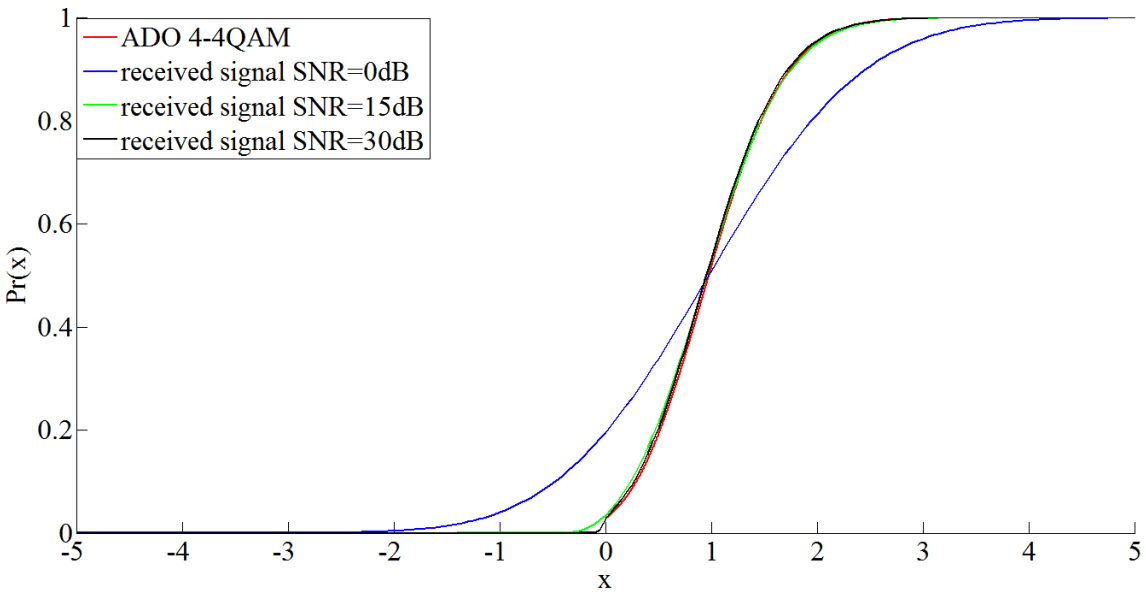

Figure 4.3 Cumulative distribution functions of transmitted and received ADO-OFDM signals with different SNRs.

In the ASCO-OFDM case (Figure 4.4), the CDF curves (red, green and black) are almost overlapped, where $\Pr(x \le 1) = 0.51$. The blue curve is the CDF when SNR=0dB, where $\Pr(x \le 1) = 0.48$. Thus, the mean value is also around 1.

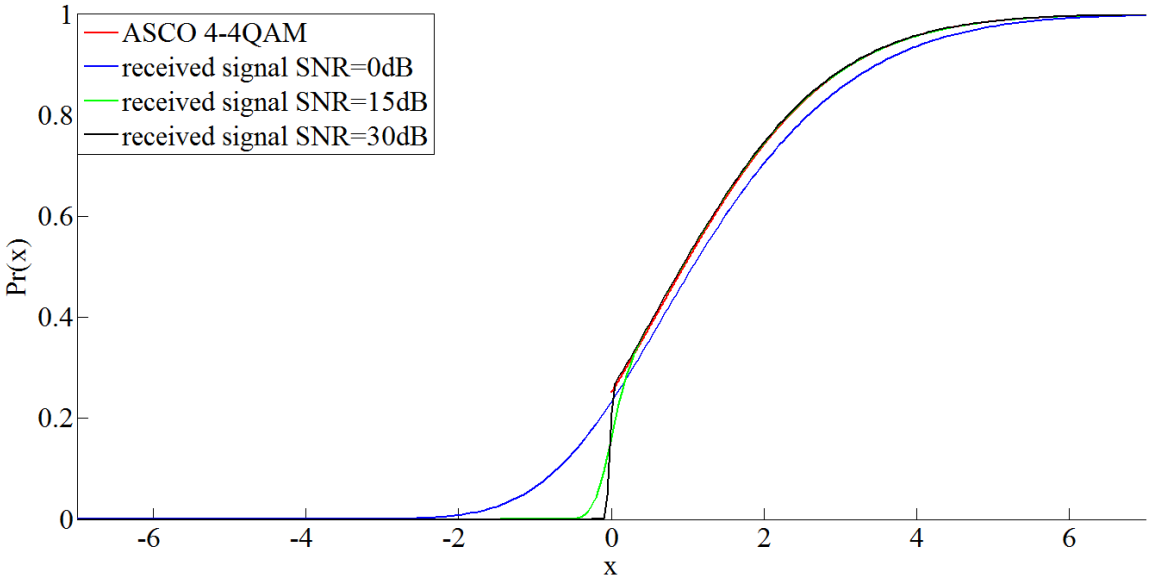

Figure 4.4 Cumulative distribution functions of transmitted and received ASCO-OFDM signals with different SNRs.

The PDF curves for both schemes are shown in Figures 4.5 and 4.6, respectively. Apparently, as the noise power decreases, the distributions of received signals (blue, green, and black) are asymptotically close to that of transmitted signals (red curve).

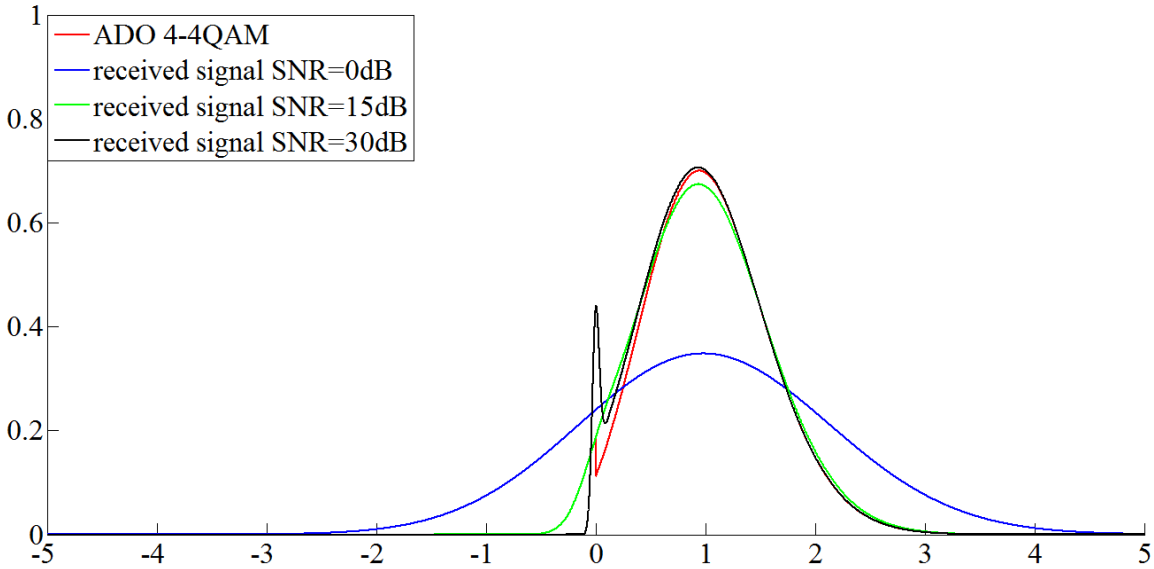

Figure 4.5 Probability density functions of transmitted and received ADO-OFDM signals with different SNRs.

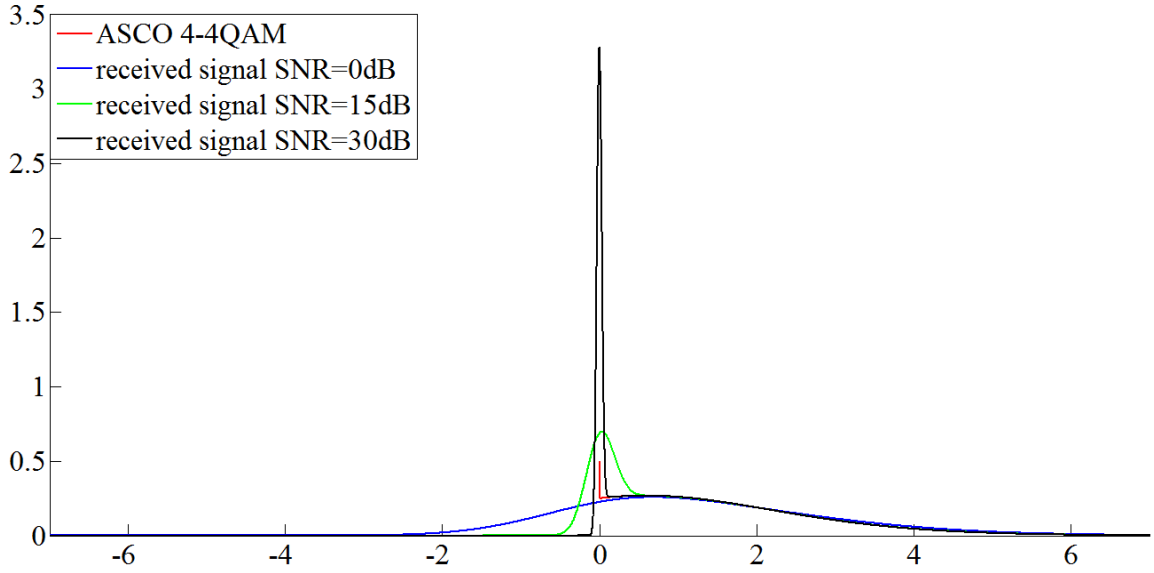

Figure 4.6 Probability density functions of transmitted and received ASCO-OFDM signals with different SNRs.

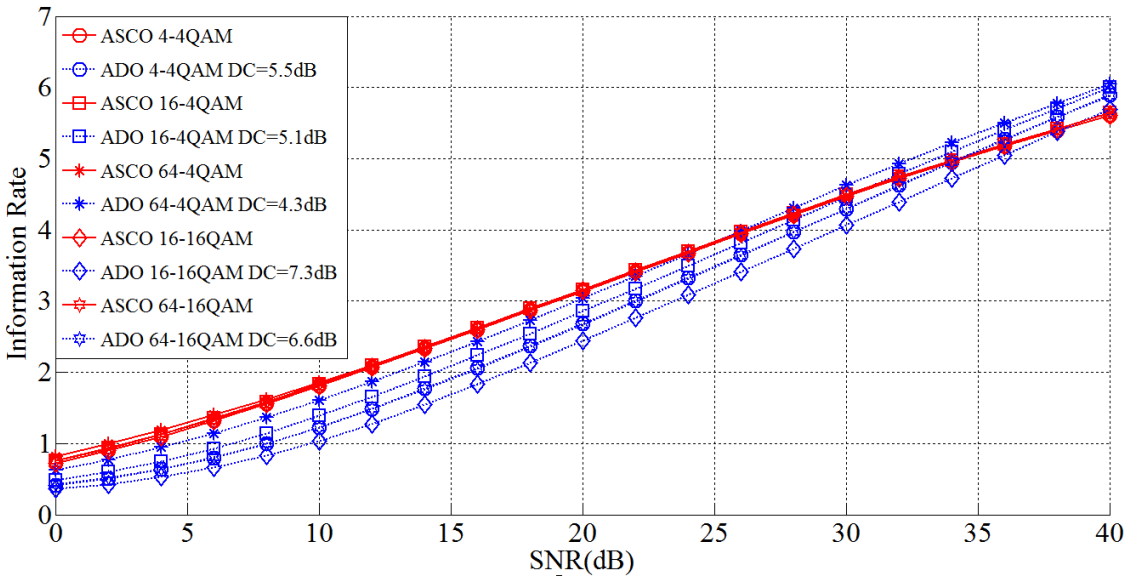

Figure 4.7 Information Rates of ADO-OFDM and ASCO-OFDM with optical power constraint for different constellation combinations.

Finally, the information rates of ADO-OFDM and ASCO-OFDM are compared in Figure 4.7. Five different constellation combinations among 4-QAM, 16-QAM, and 64-QAM are taken into account in the simulation because the odd subcarriers and the even

subcarriers can be separately modulated. This strategy does not affect the power efficiency for ASCO-OFDM, but it is important to ADO-OFDM due to the DC bias. In order to improve the power efficiency, DCO-OFDM symbols are drawn from a smaller constellation, which results in a smaller DC bias level. The DC bias values used in our simulation come from Table 2.2.

In Figure 4.7, the solid curve represents the information rate of ASCO-OFDM, and the dotted curve represents that of ADO-OFDM. Five different markers represent five different constellation combinations respectively, which are shown in the legend. The information rates of ASCO-OFDM are almost the same in different constellation cases when the average optical power is fixed. However, ADO-OFDM achieves different Information rates. Apparently, the information rate of ADO-OFDM depends on the DC bias level. In the figure, if a smaller DC bias is added, a higher information rate is achieved. For example, ADO-OFDM with 64-4QAM achieves the highest result while 16-16QAM case achieves the lowest result because they are added by the smallest and the largest DC biases, respectively.

Then we compare the information rates between ASCO-OFDM and ADO-OFDM. In Figure 4.7, ASCO-OFDM outperforms ADO-OFDM at relatively low SNRs. Compared to ADO-OFDM with 64-4 QAM, ASCO-OFDM can transmit more information in the range from 0dB to 24dB. But, ADO-OFDM has a better performance at high SNRs. Recall that each transmitted ASCO-OFDM signal has two consecutive sub-blocks, x_{ASCO}^{i} and x_{ASCO}^{j}; each transmitted ADO-OFDM signal has only one block, x_{ADO}. Because the length of x_{ASCO}^{i} and x_{ADO} is the same, we need to compare the information rate in x_{ASCO}^{i} with that in x_{ADO}. In one sub-block of ASCO-OFDM, half of

the information carried by the even subcarriers is transmitted. In ADO-OFDM, all the information on both odd and even subcarriers can be transmitted in one block. Thus, the information rate of ADO-OFDM is actually higher than that of ASCO-OFDM in the absence of noise (high SNRs). However, a transmitted signal has to be constraint to an average optical power. In ADO-OFDM, a part of optical power is consumed by the DC bias. If the transmitted signal is interfered by a large noise, the information rate will be less than that of ASCO-OFDM.

4.5 Conclusion

In this chapter, the information rates have been compared between ADO-OFDM and ASCO-OFDM in an AWGN channel. When the distribution of transmitted signals is known, the information rate of the corresponding system can be numerically obtained by calculating the mutual information with a limit on the average transmitted optical power. The performances of both schemes are compared and analyzed in the previous section. Since noises cannot be ignored in the practice and the average optical power must be limited, ASCO-OFDM is able to transmit higher information rates than ADO-OFDM.

CHAPTER 5

PERFORMANCES OF TWO-DIMENSIONAL ASYMMETRICALLY AND SYMMETRICALLY CLIPPING OPTICAL OFDM IN AWGN

In the future, IM/DD optical wireless systems can be easily employed to provide a high speed wireless transmission service in an indoor environment. So far, many different kinds of IM/DD optical wireless systems have been proposed, such as ADO-OFDM [8], hybrid ACO-OFDM [15], and polar-OFDM (P-OFDM) [16]. Conventionally, LEDs and photodiodes are used to realize the transmission and reception. In practice, the transmitter and the receiver will be designed as an array of LEDs and photodiodes. However, most experiments are developed over single-input single-output (SISO) systems. In the meantime, two-dimensional (2D) optical wireless systems, which are a form of multiple-input multiple-output (MIMO) systems, also have been studied in [26-28], and they are getting more and more attention.

The two most popular modulation schemes, DC biased optical (DCO)-OFDM [4] and asymmetrically clipping optical (ACO)-OFDM [5], have been used to make real and non-negative signals in one-dimensional (1D) optical wireless systems. Also, these two schemes have been investigated in 2D optical wireless systems. A 2D DC biased optical (DCO)-OFDM has been studied in [26-28]. However, DCO-OFDM is not optical power efficient, and the performance highly depends on the DC bias level in 1D OWC [10]. ACO-OFDM is much more optically power efficient than DCO-OFDM, but it requires twice the bandwidth of the DCO-OFDM. In addition, ACO-OFDM transmitted signals inherently have a large peak-to-average power ratio (PAPR). The 2D ACO-OFDM has been discussed in [29]. In order to improve the bandwidth efficiency and reduce the

PAPR, ADO-OFDM was proposed recently. The ACO-OFDM scheme is used to modulate the odd subcarriers, and the DCO-OFDM scheme is used to modulate the even subcarriers. However, the performances of ADO-OFDM are still affected by the DC bias level. In Chapter 2, we have proposed an optical wireless system without adding a DC bias, called asymmetrically and symmetrically clipping optical (ASCO)-OFDM. Compared with ADO-OFDM, it requires much less optical power to transmit each bit. Equivalently, ASCO-OFDM has a higher bit rate than does ADO-OFDM when the same optical power is supplied. In Chapter 4, we have investigated the information rates of both systems. The simulation results show that if the larger DC bias is added, the lower information rate is achieved for ADO-OFDM. Moreover, the information rate of ADO-OFDM is lower than that of ASCO-OFDM in a large range of low SNRs. Thus, ADO-OFDM will not be considered as a competitive scheme any more. In this chapter, we apply ASCO-OFDM into 2D IM/DD optical systems and investigate the performances in terms of bandwidth efficiency, peak-to-average power ratio (PAPR) and symbol error rate (SER) [30].

5.1 Two-Dimensional ACO-OFDM

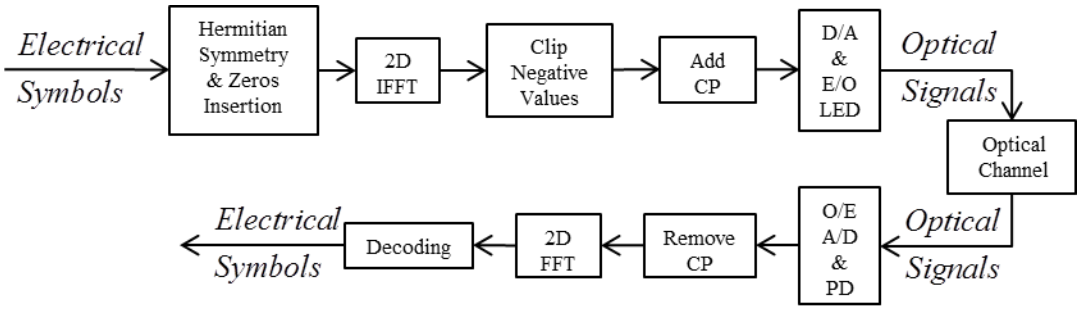

Figure 5.1 Structure of two-dimensional (2D) ACO-OFDM system.

The block diagram of a 2D ACO-OFDM system is shown in Figure 5.1. Blocks of electrical symbols drawn from the constellations, such as 4-QAM, 16-QAM, and 64-QAM, are input to the system. Conventionally, the symbols are mapped into a signal vector in 1D optical wireless system. In the 2D case, the input symbols are mapped into a $N_1 \times N_2$ signal matrix as follows:

$$S_{N_1 \times N_2} = \begin{bmatrix} S_{0,0} & S_{0,1} & \cdots & S_{0,N_2-1} \\ S_{1,0} & S_{1,1} & \cdots & S_{1,N_2-1} \\ \vdots & \vdots & \ddots & \vdots \\ S_{N_1-1,0} & S_{N_1-1,1} & \cdots & S_{N_1-1,N_2-1} \end{bmatrix} \tag{5.1}$$

where N_1 and N_2 are even numbers. This matrix is taken by a 2D IFFT to transform it into the time domain to yield,

$$s_{N_1 \times N_2} = \begin{bmatrix} s_{0,0} & s_{0,1} & \cdots & s_{0,N_2-1} \\ s_{1,0} & s_{1,1} & \cdots & s_{1,N_2-1} \\ \vdots & \vdots & \ddots & \vdots \\ s_{N_1-1,0} & s_{N_1-1,1} & \cdots & s_{N_1-1,N_2-1} \end{bmatrix} \tag{5.2}$$

The upper cases represent frequency domain symbols and the lower cases represent time domain signals. In order to ensure each value in the matrix *s* real, the elements in matrix S must have 2D Hermitian symmetry constraint, which is defined as follows:

$$S(k_1,k_2)=S^*(N_1-1-k_1,N_2-1-k_2) \tag{5.3}$$

Thus, the elements $S_{0,n}$ in the first row and the elements $S_{m,0}$ in the first column are set to be zeroes. Another element $S_{N_1/2,N_2/2}$, which corresponds to $S_{0,0}$, has to be zero as well. Then, symbols are put onto the odd columns (odd rows); zeroes are set to the rest even columns (even rows). Since the transmitted optical signals are 2D frames, we can use either odd columns or odd rows to carry symbols. If symbols are on the odd columns, the elements in s have the property that $s_{m,n}=-s_{m,N_2/2+n}$. Similarly, if symbols are on the odd rows, the elements in s have the property that $s_{m,n}=-s_{N_1/2+m,n}$. In order to obtain the non-negative signals, the negative values in $s_{N_1\times N_2}$ should be clipped to zeroes because $s_{m,n}$ is real but bipolar. The transmitted signal is given by

$$x_{m,n}=0.5(s_{m,n}+|s_{m,n}|) \tag{5.4}$$

In 2D optical signal transmission, the cyclic prefix (CP) is added to both columns and rows of $x_{m,n}$ to mitigate the effect of misalignment, which is denoted by $\tilde{x}_{m,n}$. The intensity of each pixel in the transmitted frame is modulated by the corresponding element in $\tilde{x}_{m,n}$.

Passing through the channel h, the arrival signal is given by

$$\tilde{y}_{m,n}=\tilde{x}_{m,n}\otimes h_{m,n}+w_{m,n} \tag{5.5}$$

where $\otimes$ is 2D linear convolution. In this work, we assume that a short range optical path can be modeled as a flat fading channel so that $|h_{m,n}|$ is the same for any coordinate point. The noise $w_{m,n}$ consists of shot noise and thermal noise, which can be approximated as additive white Gaussian noise (AWGN). After removing the CP and transforming the arrival signal into the frequency domain, the amplitude of each symbol on the odd columns is reduced by half due to the clipping approach. The symbols appearing on the even columns are the ACO-OFDM clipping noise. The information can be easily recovered by only detecting the symbols on the odd columns.

5.2 Two-Dimensional ASCO-OFDM

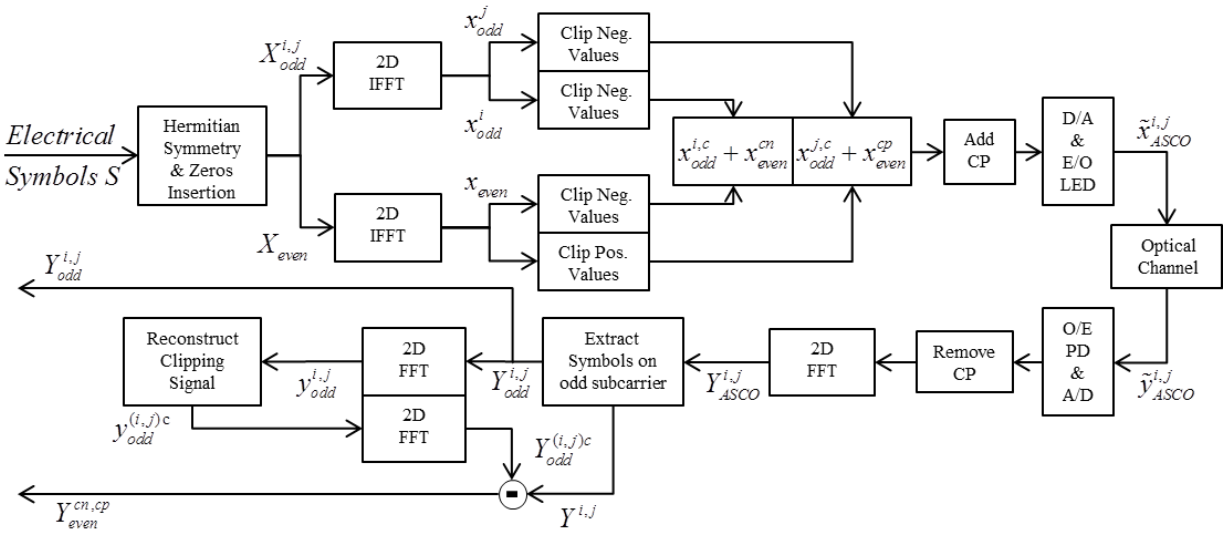

Figure 5.2 Structure of two-dimensional 2D ASCO-OFDM system.

In this section, we describe the structure of 2D ASCO-OFDM optical wireless system, which is presented in Figure 5.2. The input symbols are parsed into three parts, and then they are mapped into three $N_1 \times N_2$ matrices**,** X_{odd}^{i}, X_{odd}^{j} and X_{even}. The symbols are put onto the odd columns and the even columns respectively, which are shown as follows:

$$X_{odd} = \begin{bmatrix} 0 & 0 & 0 & 0 & \cdots & 0 & 0 \\ 0 & S_{1,1} & 0 & S_{1,3} & \cdots & 0 & S_{1,N_2-1} \\ 0 & S_{2,1} & 0 & S_{2,3} & \cdots & 0 & S_{2,N_2-1} \\ \vdots & \vdots & \vdots & \vdots & \ddots & \vdots & \vdots \\ 0 & S_{N_1-1,1} & 0 & S_{N_1-1,3} & \cdots & 0 & S_{N_1-1,N_2-1} \end{bmatrix} \tag{5.6}$$

$$X_{even} = \begin{bmatrix} 0 & 0 & 0 & 0 & \cdots & 0 & 0 \\ 0 & 0 & S_{1,2} & 0 & \cdots & S_{1,N_2-2} & 0 \\ 0 & 0 & S_{2,2} & 0 & \cdots & S_{2,N_2-2} & 0 \\ \vdots & \vdots & \vdots & \vdots & \ddots & \vdots & \vdots \\ 0 & 0 & S_{N_1-1,2} & 0 & \cdots & S_{N_1-1,N_2-2} & 0 \end{bmatrix} \tag{5.7}$$

i and j represent two consecutive time slots. X_{odd}^{i}, X_{odd}^{j} and X_{even} are constraint to 2D Hermitian symmetry. They can be transformed by a 2D IFFT to obtain real but bipolar matrices x_{odd}^{i}, x_{odd}^{j}, and x_{even}. In order to make the matrices real and unipolar, all the negative elements of x_{odd}^{i} and x_{odd}^{j} have to be clipped to zeroes to yield $x_{odd}^{i,c}$ and $x_{odd}^{j,c}$. We use c to indicate the clipped signal. $x_{odd}^{i,c}$, $x_{odd}^{j,c}$ are two independent signals, which are given by

$$x_{odd}^{i,c} = 0.5(x_{odd}^{i} + \left| x_{odd}^{i} \right|) \tag{5.8}$$

$$x_{odd}^{j,c} = 0.5(x_{odd}^{j} + \left| x_{odd}^{j} \right|) \tag{5.9}$$

They are transmitted in two consecutive sub-blocks, i and j. If an OFDM signal is converted from only even columns, such as X_{even}, the element in the matrix x_{even} has the property that $s_{m,n} = s_{m,N_2/2+n}$. Thus, half of the information in x_{even} is lost because of

clipping. In order to make all the information in x_{even} transmitted, we generate two different clipped signal matrices for x_{even} : x_{even}^{cn} is obtained by clipping the negative elements to zeroes and keeping the positive elements; x_{even}^{cp} is obtained by clipping the positive elements to zeroes and turn the sign of negative elements to positive. x_{even}^{cn} and x_{even}^{cp} are respectively given by

$$x_{even}^{cn} = 0.5(x_{even} + |x_{even}|) \tag{5.10}$$

$$x_{even}^{cp} = 0.5(-x_{even} + |x_{even}|) \tag{5.11}$$

These two signal matrices, x_{even}^{cn} and x_{even}^{cp}, are transmitted in two consecutive time slots and they will be respectively added to $x_{odd}^{i,c}$ and $x_{odd}^{j,c}$ as follows:

$$x_{ASCO}^{i} = x_{odd}^{i,c} + x_{even}^{cn} \tag{5.12}$$

$$x_{ASCO}^{j} = x_{odd}^{j,c} + x_{even}^{cp} \tag{5.13}$$

Thus, a transmitted ASCO-OFDM signal consists of two parts of signals, x_{ASCO}^{i} and x_{ASCO}^{j}. CPs are attached to x_{ASCO}^{i} and x_{ASCO}^{j} to mitigate the effect of misalignment, which are denoted by $\tilde{x}_{ASCO}^{i}$ and $\tilde{x}_{ASCO}^{j}$. After removing the CP, the arrival signals, y_{ASCO}^{i} and y_{ASCO}^{j}, can be respectively given by

$$\begin{aligned} y_{ASCO}^{i} &= x_{ASCO}^{i} \otimes h + w^{i} \\ &= (x_{odd}^{i,c} + x_{even}^{cn}) \otimes h + w^{i} \end{aligned} \tag{5.14}$$

$$\begin{aligned} y_{ASCO}^{j} &= x_{ASCO}^{j} \otimes h + w^{j} \\ &= (x_{odd}^{j,c} + x_{even}^{cp}) \otimes h + w^{j} \end{aligned} \tag{5.15}$$

The frequency domain form of the arrival signals are given by

$$Y_{ASCO}^{i} = \hat{X}_{odd}^{i,c} + \hat{X}_{even}^{cn} + W^{i} \tag{5.16}$$

$$Y_{ASCO}^{j} = \hat{X}_{odd}^{j,c} + \hat{X}_{even}^{cp} + W^{j} \tag{5.17}$$

$\hat{X}_{odd}^{i,c}$, $\hat{X}_{even}^{cn}$, $\hat{X}_{odd}^{j,c}$ and $\hat{X}_{even}^{cp}$ represent the detected matrices of symbols respectively. For $\hat{X}_{odd}^{i,c}$ or $\hat{X}_{odd}^{j,c}$, it is observed that the original symbols of X_{odd}^{i} or X_{odd}^{j} are on the odd columns, but their amplitudes are reduced by half; the clipping noise appear on the even columns where should be zeroes before clipping. The clipping noise has been proved that they are the FFT of the absolute version of $\left|x_{odd}^{i}\right|$ [10]. Thus, in order to recover X_{odd}^{i} or X_{odd}^{j}, we directly detect the symbols on the odd columns without considering the clipping noise. However, the clipping noise can be used to improve the SER performance [10, 20]. For $\hat{X}_{even}^{cn}$ or $\hat{X}_{even}^{cp}$, the original symbols on the even columns are severely interfered due to the clipping. We expand the Equations (5.16) and (5.17) as follows,

$$Y_{ASCO}^{i} = 0.5(\hat{X}_{odd}^{i} + \left|\hat{X}_{odd}^{i}\right| + \hat{X}_{even} + \left|\hat{X}_{even}\right|) + W^{i} \tag{5.18}$$

$$Y_{ASCO}^{j} = 0.5(\hat{X}_{odd}^{j} + \left|\hat{X}_{odd}^{j}\right| - \hat{X}_{even} + \left|\hat{X}_{even}\right|) + W^{i} \tag{5.19}$$

Thus, in the absence of noise, the symbols located on the odd columns and even columns are shown respectively as,

$$Y_{odd,ASCO}^{i} = 0.5\hat{X}_{odd}^{i} \tag{5.20}$$

$$Y_{even,ASCO}^{i} = 0.5(\left|\hat{X}_{odd}^{i}\right| + \hat{X}_{even} + \left|\hat{X}_{even}\right|) \tag{5.21}$$

$$Y_{odd,ASCO}^{j} = 0.5\hat{X}_{odd}^{j} \tag{5.22}$$

$$Y_{even,ASCO}^{j} = 0.5(\left|\hat{X}_{odd}^{j}\right| - \hat{X}_{even} + \left|\hat{X}_{even}\right|) \tag{5.23}$$

By using the estimated symbols $0.5\hat{X}_{odd}^{i}$ and $0.5\hat{X}_{odd}^{j}$, we can reconstruct the clipping noises, (absolute version of original symbols), $0.5\left|\hat{X}_{odd}^{i}\right|$ and $0.5\left|\hat{X}_{odd}^{j}\right|$. The clipping noises will be removed from the even columns, and then the rest symbols in two matrices are given by

$$\hat{X}_{even}^{cn} = 0.5(\hat{X}_{even} + \left|\hat{X}_{even}\right|) \tag{5.24}$$

$$\hat{X}_{even}^{cp} = 0.5(-\hat{X}_{even} + \left|\hat{X}_{even}\right|) \tag{5.25}$$

Finally, the original symbols carried on the even columns are obtained by subtracting $\hat{X}_{even}^{cp}$ from $\hat{X}_{even}^{cn}$,

$$\hat{X}_{even} = \hat{X}_{even}^{cn} - \hat{X}_{even}^{cp} \tag{5.26}$$

5.3 Performance Analysis and Simulation Results

In this section, we compare the performances between 2D ASCO-OFDM and 2D ACO-OFDM in terms of Peak-to-average ration (PAPR), average bit rate, and symbol error ratio (SER). Since the transmitted signals are intensity varying light, the average optical power is defined by $E\{x(n_1, n_2)\}$.

5.3.1 Peak-to-average Power Ratio

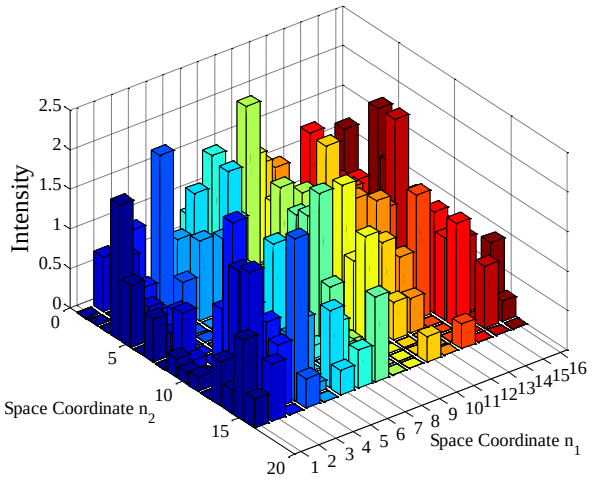

Figure 5.3 Three-Dimensional **(**3D) view of a 2D ACO-OFDM signal frame.

In Figure 5.3, we present a size of 16×16 2D ACO-OFDM signal frame. The intensity of each pixel is plotted against the 2D coordinate n_1 and n_2. The original symbols are drawn from 4-QAM and they are converted by a 2D IFFT into the time domain. Since the output of 2D IFFT follows Gaussian distribution with mean zero and variance σ, the PDF of an

ACO-OFDM signal follows clipped Gaussian distribution with mean $\sigma/\sqrt{2\pi}$ and variance $\sigma^2/2$.

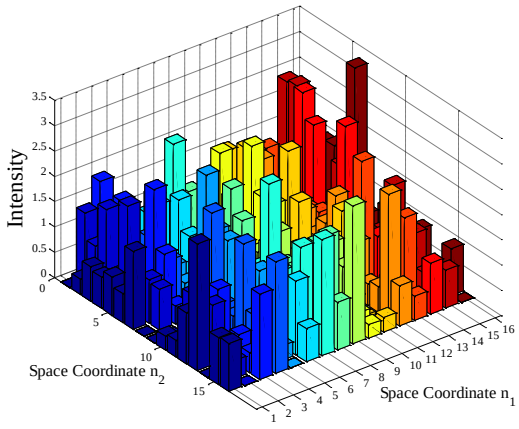

Figure 5.4 Three-Dimensional (3D) view of a 2D ASCO-OFDM signal frame.

Figure 5.4 shows a 16×16 2D ASCO-OFDM signal frame where the symbols are drawn from 4-QAM. This signal frame represents the transmitted signal $x_{ASCO}^{i} = x_{odd}^{i,c} + x_{even}^{cn}$. Because both $x_{odd}^{i,c}$ and x_{even}^{cn} are clipped signals, they follow the clipped Gaussian distribution as well. The PDF of x_{ASCO}^{i} is the convolution of two clipped Gaussian distributions, which is presented in [9]. The mean and variance of x_{ASCO}^{i} is $2\sigma/\sqrt{2\pi}$ and $(\pi-1)\sigma^2/\pi$, respectively, where σ is the variance of x_{odd}^{i} and x_{even}. Note that the mean of x_{ASCO}^{i} is twice as large as that of x_{ACO} while the peak value is not doubled. Therefore, we believe that 2D ASCO-OFDM has lower PAPR than 2D ACO-OFDM.

The PAPR performances of 2D ASCO-OFDM and 2D ACO-OFDM with different constellations are compared in Figure 5.5. The red solid curves represent the

PAPR of ACO-OFDM and the blue dashed curves represent the PAPR of ASCO-OFDM. We use circle, square and star to represent the ACO-OFDM signals modulated by 4-QAM, 16-QAM, and 64-QAM, respectively. Since ACO-OFDM signals and SCO-OFDM signals are independent, they can be modulated by different constellations. In order to fairly compare the PAPR between two transmitted signals, the same constellation is applied onto odd and even subcarriers for 2D ASCO-OFDM. We notice that the PAPR of 2D ASCO-OFDM is 2dB less than that of 2D ACO-OFDM.

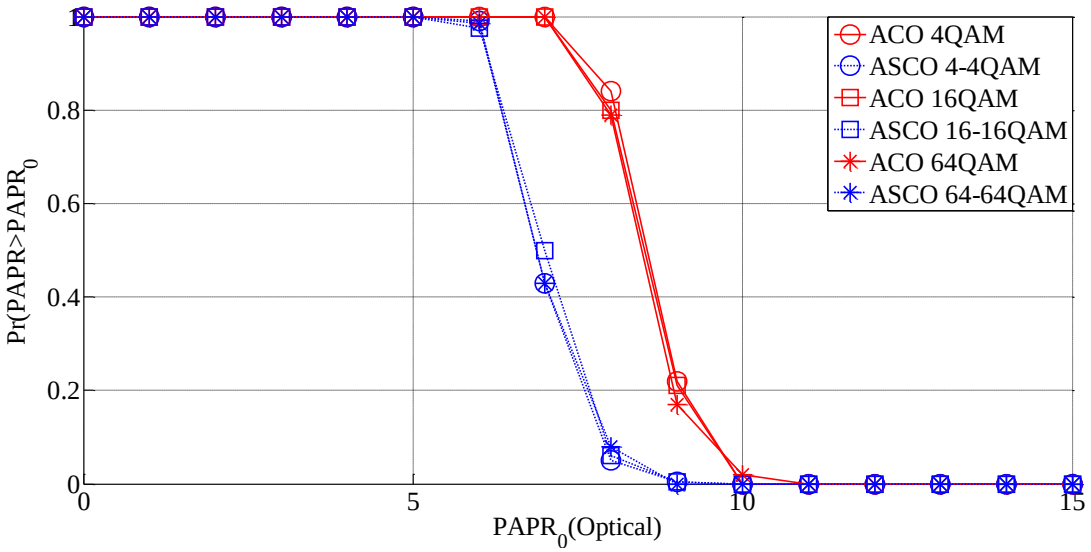

Figure 5.5 PAPR (Optical Power) Comparisons of 2D ASCO-OFDM and 2D ACO-OFDM.

5.3.2 Spectral Efficiency and Average Bit Rate

In the 2D ACO-OFDM scheme, $0.5N_2(N_1-1)$ symbols are mapped into a $N_1 \times N_2$ matrix; hence the spectral efficiency of 2D ACO-OFDM is given by $0.5(N_1-1)/N_1$. In order to improve the spectral efficiency, not only the odd columns but also the even columns are used to carry symbols in the 2D ASCO-OFDM scheme. In each frame, $0.5N_2(N_1-1)$ symbols are carried by the odd columns and $(0.5N_2-1)(N_1-1)-1$ symbols

are carried by the even columns; hence the spectral efficiency of 2D ASCO-OFDM is given by $[(N_2-1)(N_1-1)-1]/N_1N_2$. For large N_1 and N_2, the spectral efficiency of 2D ASCO-OFDM is twice as larger as that of 2D ACO-OFDM and it is close to 1.

In ACO-OFDM, only the odd columns are used to carry symbols; thus, the average bit rate of 2D ACO-OFDM can be calculated by $(\log_2 C_{ACO})/2$, where C_{ACO} is the constellation size of ACO-OFDM symbols. In 2D ASCO-OFDM, symbols carried on odd and even columns are drawn from different constellations because odd columns are modulated by ACO-OFDM while even columns are modulated by SCO-OFDM. Note that all the information carried on even columns is separated into two consecutive time slots. Thus, half of the information in X_{even} is transmitted by even columns in one frame, x^i_{ASCO} or x^j_{ASCO}. Therefore, the average bit rate of 2D ASCO-OFDM for one frame can be obtained by $(\log_2 C_{ACO}+0.5\log_2 C_{SCO})/2$, where C_{ACO} and C_{SCO} are similarly defined. The average bit rates for both schemes with different constellations are compared in Table 5.1.

5.3.3 Symbol Error Rate

We compare the symbol error rate (SER) vs. SNR for 2D ASCO-OFDM and 2D ACO-OFDM in Figure 5.6. The solid curves represent 2D ACO-OFDM system and the dashed curves represent 2D ASCO-OFDM system. 2D ACO-OFDM transmitted frames are modulated by 4-QAM, 16-QAM and 64-QAM, respectively. 2D ASCO-OFDM are investigated in the constellation combinations of 4-4QAM, 16-4QAM, and 64-4QAM Compared the solid curves to the dashed curves with the same marker, the SER performance of 2D ASCO-OFDM is worse than that of 2D ACO-OFDM. The 2D ASCO-

TABLE 5.1 Average Bit Rates of ACO-OFDM and ASCO-OFDM with Different Constellation Combinations

	ACO-OFDM		ASCO-OFDM
ACO-OFDM 4-QAM	1	ACO-OFDM 4-QAM SCO-OFDM 4-QAM	1.5
ACO-OFDM 16-QAM	2	ACO-OFDM 4-QAM SCO-OFDM 16-QAM	2
ACO-OFDM 64-QAM	3	ACO-OFDM 16-QAM SCO-OFDM 4-QAM	2.5
		ACO-OFDM 16-QAM SCO-OFDM 16-QAM	3
		ACO-OFDM 64-QAM SCO-OFDM 4-QAM	3.5

OFDM scheme is interfered by much more noise because both the odd columns and the even columns are used to carry symbols. Additionally, the detection procedure of SCO-OFDM symbols depends on the detected ACO-OFDM symbols. However, the average bit rates of 2D ACO-OFDM with 4-QAM, 16-QAM and 64-QAM differ from that of 2D ASCO-OFDM with 4-4QAM, 16-4QAM and 64-4QAM. Thus, we present the SER comparisons of the two schemes with the same bit rate, such as 2D ACO-OFDM with 16-QAM vs. 2D ASCO-OFDM with 4-16QAM, 2D ACO-OFDM with 64-QAM vs. 2D ASCO-OFDM with 16-16QAM. The SER performance of 2D ASCO-OFDM with 4-16QAM is represented by the dashed diamond curves and it is close to that of 2D ACO-OFDM with 16-QAM. The SER performance of 2D ASCO-OFDM with 16-16QAM is

represented by the dashed pentagram curves and it outperforms 2D ACO-OFDM with 64-QAM. Moreover, we could apply larger constellations onto the odd columns, the even columns or both to achieve higher bit rate.

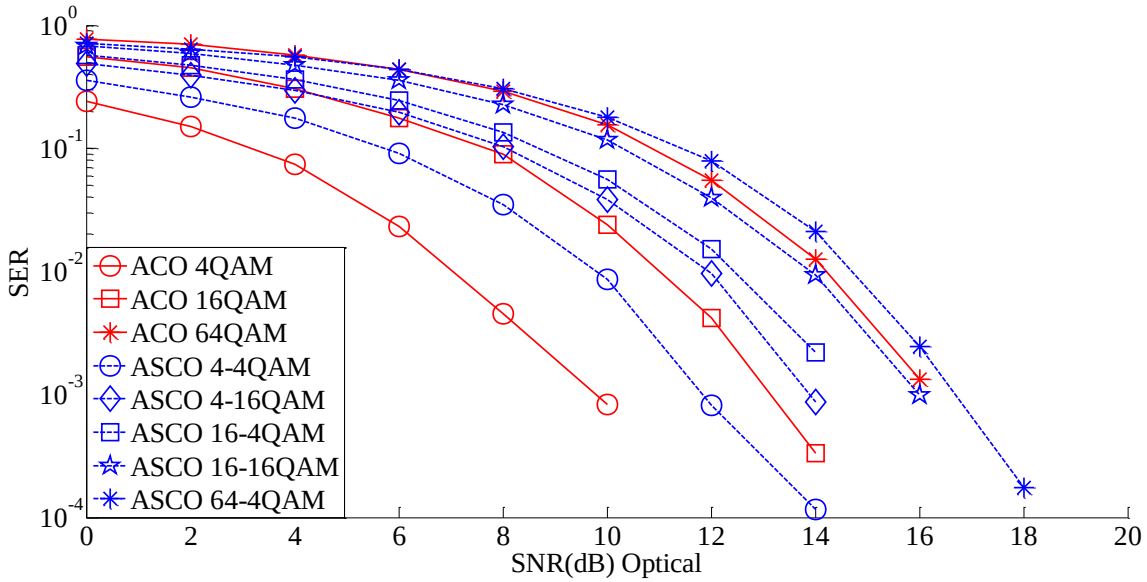

Figure 5.6 SER Comparisons of 2D ASCO-OFDM and 2D ACO-OFDM with different constellation combinations.

5.4 Conclusion

In this chapter, we successfully apply an ASCO-OFDM scheme into 2D IM/DD optical wireless systems. It improves the spectrum efficiency because both the odd columns and the even columns are used to carry symbols; only the odd columns are modulated in the 2D ACO-OFDM scheme. Since the odd columns and the even columns of 2D ASCO-OFDM can be separately detected, different constellation combinations are taken into account for modulation. By applying modest constellation size, 2D ASCO-OFDM can achieve a higher bit rate than 2D ACO-OFDM with 64-QAM. The 2D ASCO-OFDM is more power efficient because its PAPR performance is 2dB lower than that of 2D ACO-

OFDM. The last but not the least, the SER of 2D ASCO-OFDM is acceptable when the average bit rate is the same. Consequently, ASCO-OFDM is the most attractive choice for 2D IM/DD optical wireless systems.

APPENDIX A

THE PROPERTY OF OFDM SYMBOLS CONVERTED FROM ONLY EVEN SUBCARRIERS

In order to explicitly understand the characteristic of OFDM symbols only carried by even subcarriers, please refer to the following derivation. The IDFT of a length-2N frequency domain sequence $X(k)$ is defined by

$$x(n) = \frac{1}{2N} \sum_{k=0}^{2N-1} X(k) \exp(\frac{j2\pi nk}{2N}) \tag{A.1}$$

In order to present Equation (A.1) by the sum of the odd subcarriers and the even subcarriers, we use a new index l instead of k,

$$x(n) = \frac{1}{2N} \sum_{l=0}^{N-1} X(2l) \exp(\frac{j2\pi n2l}{2N}) + \frac{1}{2N} \sum_{l=0}^{N-1} X(2l+1) \exp(\frac{j2\pi n(2l+1)}{2N}) \tag{A.2}$$

If the odd subcarriers of $X(k)$ are set to zero, then the second term of Equation (A.2) is equal to zero. Thus $x(n)$ is given by

$$x(n) = \frac{1}{2N} \sum_{l=0}^{N-1} X(2l) \exp(\frac{j2\pi n2l}{2N}) \tag{A.3}$$

Then we calculate $x(n+N)$. Substituting the index $n+N$ into Equation (A.3), we have

$$\begin{aligned} x(n+N) &= \frac{1}{2N}\sum_{l=0}^{N-1} X(2l)\exp(\frac{j2\pi(n+N)2l}{2N}) \\ &= \frac{1}{2N}\sum_{l=0}^{N-1} X(2l)\exp(\frac{j2\pi n2l}{2N})\exp(\frac{j2\pi N2l}{2N}) \end{aligned} \tag{A.4}$$

Note that the second exponential term can be simplified to $\exp(j2\pi l),\quad (l=0,1,\cdots,N-1)$, which is equal to one. Therefore, we prove that an OFDM symbol converted from only even subcarriers achieves the property that $x(n)=x(n+N)$

APPENDIX B

THE PROPERTY OF SCO-OFDM CLIPPING NOISE

In this section, we demonstrate the effect of clipping noise caused by generating SCO-OFDM signals. Supposing $x(n)$ is an SCO-OFDM signal of length 2N, then the DFT of $x(n)$ is given by

$$\begin{aligned} X(k) &= \sum_{n=0}^{2N-1} x(n)\exp(\frac{-j2\pi nk}{2N}) \\ &= \sum_{\substack{n=0 \\ x(n)>0}}^{N-1} x(n)\exp(\frac{-j2\pi nk}{2N}) + x(n+N)\exp(\frac{-j2\pi(n+N)k}{2N}) \\ &\quad + \sum_{\substack{n=0 \\ x(n)<0}}^{N-1} x(n)\exp(\frac{-j2\pi nk}{2N}) + x(n+N)\exp(\frac{-j2\pi(n+N)k}{2N}) \end{aligned} \tag{B.1}$$

The exponential term $\exp(\frac{-j2\pi(n+N)k}{2N})$ is equal to $\exp(\frac{-j2\pi nk}{2N})\exp(-j\pi k)$, and the value of $\exp(-j\pi k)$ is given by

$$\exp(-\mathrm{j}\pi k) = \begin{cases} 1, k \text{ is even} \\ -1, k \text{ is odd} \end{cases} \tag{B.2}$$

By using the property of $x(n) = x(n+N)$ and substituting Equation (B.2) into Equation (B.1), we obtain that

$$X(k)=\begin{cases}2\sum\limits_{\substack{n=0\\x(n)>0}}^{N-1}x(n)\exp(\frac{-j2\pi nk}{2N})+2\sum\limits_{\substack{n=0\\x(n)<0}}^{N-1}x(n)\exp(\frac{-j2\pi nk}{2N}), & k\ is\ even\\ 0, & k\ is\ odd\end{cases} \tag{B.3}$$

After clipping, the SCO-OFDM symbols on the odd and even subcarriers are respectively shown as

$$X^{C}(k)=\begin{cases}2\sum\limits_{\substack{n=0\\x(n)>0}}^{N-1}x(n)\exp(\frac{-j2\pi nk}{2N}), & k\ is\ even\\ 0, & k\ is\ odd\end{cases} \tag{B.4}$$

We notice that the symbols on the odd subcarriers are always equal to zero, and the symbols on the even subcarriers lose the second summation in Equation (B.3). Thus, we prove that the SCO-OFDM clipping noise only affects even subcarriers without distorting the data on the odd subcarriers.

APPENDIX C

THE CHARACTERISTIC FUNCTION AND MOMENTS OF ASCO-OFDM SIGNALS

The PDF of ASCO-OFDM signals can be derived by convoluting the PDFs of ACO-OFDM signals, $x_{odd}^{i,c}$ ($x_{odd}^{j,c}$), and SCO-OFDM signals, x_{even}^{cn} (x_{even}^{cp}), which are given by Equations (4.6) and (4.7), respectively. The derivation steps are shown as follows,

$$
\begin{aligned}
f_{x_{ASCO}^{j}}(\chi) &= \int_{-\infty}^{\infty} f_{x_{odd}^{i,c}}(\alpha) f_{x_{even}^{cn}}(\chi-\alpha)d\alpha \\
&= \int_{-\infty}^{\infty} [\frac{1}{\sqrt{2\pi}\sigma_A} e^{-\frac{\alpha^2}{2\sigma_A^2}} u(\alpha) + \frac{1}{2}\delta(\alpha)] \\
&\bullet [\frac{1}{\sqrt{2\pi}\sigma_S} e^{-\frac{(\chi-\alpha)^2}{2\sigma_S^2}} u(\chi-\alpha) + \frac{1}{2}\delta(\chi-\alpha)]d\alpha \\
&= \int_{-\infty}^{\infty} \frac{1}{2\pi\sigma_A\sigma_S} e^{-\frac{\alpha^2}{2\sigma_A^2}} e^{-\frac{(\chi-\alpha)^2}{2\sigma_S^2}} u(\alpha)u(\chi-\alpha)d\alpha \\
&+ \int_{-\infty}^{\infty} \frac{1}{2\sqrt{2\pi}\sigma_A} e^{-\frac{\alpha^2}{2\sigma_A^2}} u(\alpha)\delta(\chi-\alpha)d\alpha \\
&+ \int_{-\infty}^{\infty} \frac{1}{2\sqrt{2\pi}\sigma_S} e^{-\frac{(\chi-\alpha)^2}{2\sigma_S^2}} \delta(\alpha)u(\chi-\alpha)d\alpha \\
&+ \int_{-\infty}^{\infty} \frac{1}{4}\delta(\alpha)u(\chi-\alpha)d\alpha \\
&= \frac{1}{2\sqrt{2\pi(\sigma_A^2+\sigma_S^2)}} \exp(\frac{-\chi^2}{2(\sigma_A^2+\sigma_S^2)})[erf(\frac{\sigma_A\chi}{\sigma_S\sqrt{2(\sigma_A^2+\sigma_S^2)}}) + erf(\frac{\sigma_S\chi}{\sigma_A\sqrt{2(\sigma_A^2+\sigma_S^2)}})] \\
&+ [\frac{1}{2\sqrt{2\pi\sigma_A^2}} \exp(\frac{-\chi^2}{2\sigma_A^2}) + \frac{1}{2\sqrt{2\pi\sigma_S^2}} \exp(\frac{-\chi^2}{2\sigma_S^2})]u(\chi) + \frac{1}{4}\delta(\chi)
\end{aligned}
\tag{C.1}
$$

In mathematics, the first moment, which is the mean, of this PDF is given by

$$M_1 = \int_{-\infty}^{\infty} \chi f_{x_{ASCO}^i}(\chi) d\chi = (\sigma_A + \sigma_S) / \sqrt{2\pi} \tag{C.2}$$

The mean is the average optical power of ASCO-OFDM signals. The second moment is also given by,

$$M_2 = \int_{-\infty}^{\infty} \chi^2 f_{x_{ASCO}^i}(\chi) d\chi = \frac{\sigma_A^2 + \sigma_S^2}{2} + \frac{\sigma_A \sigma_S}{\pi} \tag{C.3}$$

Then, the variance of x_{ASCO}^i is equal to $M_2 - M_1^2 = (\pi - 1)(\sigma_A^2 + \sigma_S^2)/2\pi$. If the variance of ACO-OFDM and SCO-OFDM signals are the same, i.e. $\sigma_A = \sigma_S = \sigma$, then the PDF has been presented by Equation (2.27), which is shown as the following:

$$f(\chi) = [\frac{1}{2\sqrt{\pi}\sigma} e^{-\frac{\chi^2}{4\sigma^2}} erf(\frac{\chi}{2\sigma}) + \frac{1}{\sqrt{2\pi}\sigma} e^{-\frac{\chi^2}{2\sigma^2}}] u(\chi) + \frac{1}{4}\delta(\chi) \tag{C.4}$$

where the mean and variance are $2\sigma / \sqrt{2\pi}$ and $\sigma^2(\pi - 1)/\pi$, respectively.

APPENDIX D

THE DISTRIBUTION OF THE DIFFERENCE BETWEEN TWO CLIPPED GAUSSIAN DISTRIBUTIONS

We prove that the difference between two clipped Gaussian distributions follows a normal distribution. If both x_{odd}^{i} and x_{odd}^{j} follows the same normal distribution, $N(0,\sigma)$, then $x_1 \in \left|x_{odd}^{i}\right|$ and $x_2 \in \left|x_{odd}^{j}\right|$ also follow the same distribution (called half-normal distribution) [21], and the probability density functions (PDF) are respectively given by

$$f(x_1) = \frac{\sqrt{2}}{\sigma\sqrt{\pi}} \exp(-\frac{x_1^2}{2\sigma^2}), \quad x_1 > 0 \tag{D.1}$$

$$f(x_2) = \frac{\sqrt{2}}{\sigma\sqrt{\pi}} \exp(-\frac{x_2^2}{2\sigma^2}), \quad x_2 > 0 \tag{D.2}$$

where mean is $\frac{\sigma\sqrt{2}}{\sqrt{\pi}}$ and variance is $\sigma^2(1-\frac{2}{\pi})$. If we turn the sign of x_2 to negative, then its distribution is flipped around y axis and the pdf is given by

$$f(-x_2) = \frac{\sqrt{2}}{\sigma\sqrt{\pi}} \exp(-\frac{x_2^2}{2\sigma^2}), \quad x_2 > 0 \tag{D.3}$$

with mean $-\frac{\sigma\sqrt{2}}{\sqrt{\pi}}$ and variance $\sigma^2(1-\frac{2}{\pi})$. Since $x_1 \sim N\{\frac{\sigma\sqrt{2}}{\sqrt{\pi}}, \sigma^2(1-\frac{2}{\pi})\}$ with $x_1 > 0$

and $-x_2 \sim N\{-\frac{\sigma\sqrt{2}}{\sqrt{\pi}}, \sigma^2(1-\frac{2}{\pi})\}$ with $-x_2 < 0$, the distribution of the sum $y=x_1 - x_2 \in \left|x_{odd}^i\right| - \left|x_{odd}^j\right|$ follows a normal distribution with mean zero and variance $2\sigma^2(1-\frac{2}{\pi})$, $y \in (-\infty, +\infty)$.

APPENDIX E

THE PROPERTY OF OFDM SYMBOLS CONVERTED FROM ODD OR EVEN COLUMNS IN THE TWO-DIMENSINAL OPTICAL SIGNAL MATRIX

The property of OFDM symbols mapped onto odd and even columns in the signal matrix have been derived respectively. Supposing the signal matrix is $2N_1 \times 2N_2$, the definition of two-dimensional (2D) IFFT is given by,

$$s(n,m) = \frac{1}{4N_1N_2} \sum_{k_1=0}^{2N_1-1} \sum_{k_2=0}^{2N_2-1} S(k_1,k_2) \exp[\, j(\frac{2\pi nk_1}{2N_1} + \frac{2\pi mk_2}{2N_2})] \tag{E.1}$$

In order to clearly present the summation for odd/even columns and odd/even rows, we rewrite the equation by using index l_1 and l_2 instead of k_1 and k_2,

$$\begin{aligned} s(n,m) = \frac{1}{4N_1N_2} \{ & \sum_{l_1=0}^{N_1-1} \sum_{l_2=0}^{N_2-1} S(2l_1,2l_2) \exp[\, j(\frac{2\pi n2l_1}{2N_1} + \frac{2\pi m2l_2}{2N_2})] \\ & + \sum_{l_1=0}^{N_1-1} \sum_{l_2=0}^{N_2-1} S(2l_1+1,2l_2) \exp[\, j(\frac{2\pi n(2l_1+1)}{2N_1} + \frac{2\pi m2l_2}{2N_2})] \\ & + \sum_{l_1=0}^{N_1-1} \sum_{l_2=0}^{N_2-1} S(2l_1,2l_2+1) \exp[\, j(\frac{2\pi n2l_1}{2N_1} + \frac{2\pi m(2l_2+1)}{2N_2})] \\ & + \sum_{l_1=0}^{N_1-1} \sum_{l_2=0}^{N_2-1} S(2l_1+1,2l_2+1) \exp[\, j(\frac{2\pi n(2l_1+1)}{2N_1} + \frac{2\pi m(2l_2+1)}{2N_2})]\} \end{aligned} \tag{E.2}$$

Case 1:

If the elements on the even columns are zeroes, which means only odd columns are used to carry symbols, then the output of 2D IFFT is given by

$$s(n,m)=\frac{1}{4N_1N_2}\{\sum_{l_1=0}^{N_1-1}\sum_{l_2=0}^{N_2-1}S(2l_1,2l_2+1)\exp[\,j(\frac{2\pi n2l_1}{2N_1}+\frac{2\pi m(2l_2+1)}{2N_2})] \\ +\sum_{l_1=0}^{N_1-1}\sum_{l_2=0}^{N_2-1}S(2l_1+1,2l_2+1)\exp[\,j(\frac{2\pi n(2l_1+1)}{2N_1}+\frac{2\pi m(2l_2+1)}{2N_2})]\} \tag{E.3}$$

Then we calculate $s(n,m+N_2)$. Substituting the index $m+N_2$ into Equation (E.3), we have

$$\begin{aligned}s(n,m+N_2)&=\frac{1}{4N_1N_2}\{\sum_{l_1=0}^{N_1-1}\sum_{l_2=0}^{N_2-1}S(2l_1,2l_2+1)\exp[\,j(\frac{2\pi n2l_1}{2N_1}+\frac{2\pi(m+N_2)(2l_2+1)}{2N_2})] \\ &+\sum_{l_1=0}^{N_1-1}\sum_{l_2=0}^{N_2-1}S(2l_1+1,2l_2+1)\exp[\,j(\frac{2\pi n(2l_1+1)}{2N_1}+\frac{2\pi(m+N_2)(2l_2+1)}{2N_2})]\} \\ &=\frac{1}{4N_1N_2}\{\sum_{l_1=0}^{N_1-1}\sum_{l_2=0}^{N_2-1}S(2l_1,2l_2+1)\exp[\,j(\frac{2\pi n2l_1}{2N_1}+\frac{2\pi m(2l_2+1)}{2N_2}+\frac{2\pi N_2(2l_2+1)}{2N_2})] \\ &+\sum_{l_1=0}^{N_1-1}\sum_{l_2=0}^{N_2-1}S(2l_1+1,2l_2+1)\exp[\,j(\frac{2\pi n(2l_1+1)}{2N_1}+\frac{2\pi m(2l_2+1)}{2N_2}+\frac{2\pi N_2(2l_2+1)}{2N_2})]\}\end{aligned} \tag{E.4}$$

where $\exp(\,j\frac{2\pi N_2(2l_2+1)}{2N_2})=-1$. Therefore, the relation of Case 1 between $s(n,m)$ and $s(n,m+N_2)$ is shown as

$$s(n,m)=-s(n,m+N_2) \tag{E.5}$$

Case 2:

If the elements on the odd columns are zeroes, then the signal matrix is shown as follows,

$$s(n,m)=\frac{1}{4N_1N_2}\{\sum_{l_1=0}^{N_1-1}\sum_{l_2=0}^{N_2-1}S(2l_1,2l_2)\exp[\,j(\frac{2\pi n2l_1}{2N_1}+\frac{2\pi m2l_2}{2N_2})]$$
$$+\sum_{l_1=0}^{N_1-1}\sum_{l_2=0}^{N_2-1}S(2l_1+1,2l_2)\exp[\,j(\frac{2\pi n(2l_1+1)}{2N_1}+\frac{2\pi m2l_2}{2N_2})]\} \quad \text{(E.6)}$$

Substituting the index $m+N_2$ into Equation (E.6), the result is given by the following steps,

$$\begin{aligned}s(n,m+N_2)&=\frac{1}{4N_1N_2}\{\sum_{l_1=0}^{N_1-1}\sum_{l_2=0}^{N_2-1}S(2l_1,2l_2)\exp[\,j(\frac{2\pi n2l_1}{2N_1}+\frac{2\pi(m+N_2)2l_2}{2N_2})]\\&+\sum_{l_1=0}^{N_1-1}\sum_{l_2=0}^{N_2-1}S(2l_1+1,2l_2)\exp[\,j(\frac{2\pi n(2l_1+1)}{2N_1}+\frac{2\pi(m+N_2)2l_2}{2N_2})]\}\\&=\frac{1}{4N_1N_2}\{\sum_{l_1=0}^{N_1-1}\sum_{l_2=0}^{N_2-1}S(2l_1,2l_2)\exp[\,j(\frac{2\pi n2l_1}{2N_1}+\frac{2\pi m2l_2}{2N_2}+\frac{2\pi N_2 2l_2}{2N_2})]\\&+\sum_{l_1=0}^{N_1-1}\sum_{l_2=0}^{N_2-1}S(2l_1+1,2l_2)\exp[\,j(\frac{2\pi n(2l_1+1)}{2N_1}+\frac{2\pi m2l_2}{2N_2}+\frac{2\pi N_2 2l_2}{2N_2})]\}\end{aligned} \quad \text{(E.7)}$$

where $\exp(j\frac{2\pi N_2 2l_2}{2N_2})=1$. Therefore, we obtain the relation of Case 2 between $s(n,m)$ and $s(n,m+N_2)$ is given by

$$s(n,m)=s(n,m+N_2) \quad \text{(E.8)}$$

Consequently, the relations of symbols converted from only odd or even columns between $s(n,m)$ and $s(n,m+N_2)$ have been derived.

REFERENCES

[1] K. Acolatse, Y. Bar-Ness, and S. K. Wilson, "Novel techniques of single-carrier frequency-domain equalization for optical wireless communications," *EURASIP Journal on Advances in Signal Processing* 2011: 4.

[2] D. J. F. Barros, S. K. Wilson, J. M. Kahn, "Comparison of orthogonal frequency-division multiplexing and pulse-amplitude modulation in indoor optical wireless links," *IEEE Transactions on Communications,* vol. 60, no. 1, pp. 153-163, Jan. 2012.

[3] Y. Sun, "Bandwidth-efficient wireless OFDM," *IEEE Journal on Selected Areas in Communications,* vol. 19, no. 11, pp. 2267-2278, Nov. 2001.

[4] J. Armstrong, "OFDM for optical communications," *IEEE Journal of Lightwave Technology*, vol. 27, no. 3, pp. 189-204, Feb. 2009.

[5] O. Gonzalez, R. Perez-Jimenez, S. Rodriguez, J. Rabadan, and A. Ayala, "Adaptive OFDM system for communications over the indoor wireless optical channel," *IEEE Proceedings-Optoelectronics,* vol. 153, no. 4, pp. 139-144, Aug. 2006.

[6] J. Armstrong, B. J. C. Schmidt, D. Kalra, H. A. Suraweera, and A. J. Lowery, "Performance of asymmetrically clipped optical OFDM in AWGN for an intensity modulated direct detection system," *IEEE Global Telecommunications Conference,* 2006, pp. 1-5.

[7] S. K. Wilson, J. Armstrong, "Digital modulation techniques for optical asymmetrically-clipped OFDM," *IEEE Wireless Communications and Networking Conference*, 2008, pp. 538-542.

[8] S. D. Dissanayake, J. Armstrong, "Comparison of ACO-OFDM, DCO-OFDM and ADO-OFDM in IM/DD systems," *IEEE Journal of Lightwave Technology*, vol. 31, no. 7, pp. 1063-1072, Apr. 2013.

[9] N. Wu and Y. Bar-Ness, "A novel power-efficient scheme asymmetrically and symmetrically clipping optical (ASCO)-OFDM for IM/DD optical systems," *EURASIP Journal on Advances in Signal Processing* 2015: 3.

[10] E. Katz, A. Laufer, Y. Bar-Ness, "A new improved-performance decoding technique for asymmetrically-clipped optical-OFDM," the *46th Annual Conference on Information Sciences and Systems*, 2012, pp. 1-6.

[11] J. Armstrong, B. Schmidt, "Comparison of asymmetrically clipped optical OFDM and DC-biased optical OFDM in AWGN," *IEEE Communications Letters,* vol. 12, no. 5, pp. 343-345, May 2008.

[12] J. Armstrong and A. J. Lowery, "Power efficient optical OFDM," *IEEE Electronics Letters*, vol. 42, no. 6, pp. 370-372, Mar. 2006.

[13] H. Elgala, R. Mesleh, and H. Haas, "Indoor broadcasting via white LEDs and OFDM," *IEEE Transactions on Consumer Electronics*, vol. 55, no. 3, pp. 1127-1134, Aug. 2009.

[14] H. Elgala, R. Mesleh, and H. Haas, "A study of LED nonlinearity effects on optical wireless transmission using OFDM," *the 6th International Conference on Wireless and Optical Communications Networks*, 2009, pp. 388-392.

[15] B. Ranjha, M. Kavehrad, "Hybrid asymmetrically clipped OFDM-based IM/DD optical wireless system," *IEEE/OSA Journal of Optical Communications and Networking*, vol. 6, no. 4, pp. 387-396, Apr. 2014.

[16] H. Elgala, T. D. C. Little, "P-OFDM: spectrally efficient unipolar OFDM," *Optical Fiber Communications Conference and Exhibition*, 2014, pp. 1-3.

[17] S. K. Wilson and J. Armstrong, "Transmitter and receiver methods for improving asymmetrically-clipped optical OFDM," *IEEE Transactions on Wireless Communications*, vol. 8, no. 9, pp. 4561-4567, Sep. 2009.

[18] C. Liang, B. Krongold, and J. Evans, "Performance analysis for optical OFDM transmission in short-range IM/DD systems," *IEEE Journal of Lightwave Technology*, vol. 30, no. 7, pp. 974-983, Apr. 2012.

[19] X. Li, R. Mardling, and J. Armstrong, "Channel capacity of IM/DD optical communication systems and of ACO-OFDM," *IEEE International Conference of Communications*, 2007, pp. 2128-2133.

[20] N. Wu, Y. Bar-Ness, "An improved performance decoding technique for asymmetrically and symmetrically clipped optical (ASCO)-OFDM," *the 48th Annual Asilomar Conference on Signals, Systems, and Computers,* 2014.

[21] "Half-normal distribution," Feb. 23, 2008. [Online]. Available: http://en.wikipedia.org/wiki/Half-normal_distribution [Accessed: Apr. 16, 2003].

[22] C. E. Shannon, "A mathematical theory of communication," *Bell System Technical Journal*, vol. 27, no. 4, pp. 623-656, 1948.

[23] R. You and J. M. Kahn, "Upper-bounding the capacity of optical IM/DD channels with multiple-subcarrier modulation and fixed bias using trigonometric moment space method," *IEEE Transactions on Information Theory*, vol. 48, no. 2, pp. 514-523, Feb. 2002.

[24] A. A. Farid, S. Hranilovic, "Upper and lower bounds on the capacity of wireless optical intensity channels," *IEEE International Symposium on ISIT*, 2007, pp. 2416-2420.

[25] N. Wu, Y. Bar-Ness, "Lower bounds on the channel capacity of ASCO-OFDM and ADO-OFDM," *the 49th Annual Conference on Information Sciences and Systems,* 2015.

[26] S. Hranilovic and F. R. Kschischang, "A pixelated MIMO wireless optical communication system," *IEEE Journal of Selected Topics Quantum Electronics,* vol. 12, no. 4, pp. 859-874, Jul./Aug. 2006.

[27] S. Hranilovic and F. R. Kschischang, "Short-range wireless optical communication using pixelated transmitters and imaging receivers," *IEEE International Conference on Communications,* 2004, vol. 2, pp. 891-895.

[28] M. D. A. Mohamed and S. Hranilovic, "Two-dimensional binary halftoned optical intensity channels," *IET Communications, Special Issue on Optical Wireless Communication Systems,* vol. 2, no.1, pp. 11-17, Jan. 2008.

[29] M. Rubaiyat H. Mondal, Kusha R. Panta, and J. Armstrong, "Performance of two dimensional asymmetrically clipped optical OFDM," *IEEE Globecom workshop on Optical Wireless Communications,* 2010, pp. 995-999.

[30] N. Wu, Y. Bar-Ness, "Performances of two dimensional asymmetrically and symmetrically clipped optical OFDM in AWGN," *the 49th Annual Conference on Information Sciences and Systems,* 2015.

[31] K. Acolatse, Y. Bar-Ness, and S. K. Wilson, "SCFDE with space-time coding for IM/DD optical wireless communication," *IEEE Wireless Communications and Networking Conference,* 2011, pp. 1694-1699.

[32] Z. Ghassemlooy, S. Rajbhandari, W. Popoola, *Optical Wireless Communications: System and Channel Modeling with MATLAB,* 1st ed. Boca Raton, Florida: CRC Press, 2012.